

**OPTICALLY TRANSPARENT ANTENNAS
FOR SMALL SATELLITES**

by

Jason Ramin Saberin

A thesis submitted to the faculty of
The University of Utah
in partial fulfillment of the requirements for the degree of

Master of Science

Department of Electrical and Computer Engineering

The University of Utah

August 2010

Copyright © Jason Ramin Saberlin 2010

All Rights Reserved

THE UNIVERSITY OF UTAH GRADUATE SCHOOL

SUPERVISORY COMMITTEE APPROVAL

of a Thesis submitted by

Jason Ramin Saberin

This Thesis has been read by each member of the following supervisory committee and by majority vote has been found to be satisfactory.

Chair: Cynthia Furse

Om P. Gandhi

Neal Patwari

THE UNIVERSITY OF UTAH GRADUATE SCHOOL

FINAL READING APPROVAL

To the Graduate Council of the University of Utah:

I have read the Thesis of Jason Ramin Saberin in its final form and have found that (1) its format, citations, and bibliographic style are consistent and acceptable; (2) its illustrative materials including figures, tables, and charts are in place; and (3) the final manuscript is satisfactory to the Supervisory Committee and is ready for submission to The Graduate School.

Date

Cynthia Furse
Chair, Supervisory Committee

Approved for the Major Department

Gianluca Lazzi
Chair/Dean

Approved for the Graduate Council

Charles A. Wight
Dean of The Graduate School

ABSTRACT

In this thesis the placement of antennas on a small satellite's solar cell is studied. The placement of antennas is carefully investigated by minimizing the total solar cell's power harvesting area covered by a patch antenna. Transparent antennas can potentially improve the usage of the covered area by allowing a percentage of incident solar light through. This work explores the feasibility of antennas made out of transparent oxides (TCOs) and co-planar electromagnetically coupled feeds that can be placed on solar cells. TCOs are reviewed and simplified in order to better understand material properties on antenna design. Skin depth effects are studied in detail and an empirical equation is introduced to better model skin effects resultant from thin film TCO depositions. In the second part of the thesis coupled feeds for see-through meshed antennas are studied. Properties such as antenna gain, co-polarization, efficiency and cross-polarization are discussed.

For my wife and family

CONTENTS

ABSTRACT	iii
LIST OF FIGURES	vii
LIST OF TABLES	ix
ACKNOWLEDGEMENTS	x
CHAPTERS	
1. INTRODUCTION	1
1.1 Transparent Antennas	1
1.2 Transparent Antenna Design	5
1.2.1 ITO (Indium Tin Oxide) Antennas	5
1.2.2 Meshed Patch Antennas	5
1.2.3 Integrated Solar Cell Antennas	6
1.3 Feeding Methods for Transparent Antennas	6
1.3.1 Direct Microstrip Feed	6
1.3.2 Coupled Microstrip Feed	7
1.3.3 Contributions	7
2. TRANSPARENT PATCH ANTENNAS	8
2.1 Introduction	8
2.2 Transparent Conductors	9
2.3 Skin and Ground Effects on Thin Film Microstrip Antennas	15
2.4 Analysis of TCO Effects on Patch Transparency	17
2.5 TCO and Antenna Design	19
2.6 Conclusion	23
3. PASSIVE FEED METHOD FOR MESHED MICROSTRIP PATCH ANTENNAS	25
3.1 Introduction	25
3.2 Co-planar Electromagnetically Coupled Feed	25
3.2.1 Co-Planar Coupled Feed	26
3.2.2 Inductive and Capacitive Coupling of a Passive Feed	26
3.2.3 Gap Distance and its Effects	28
3.3 Meshed See-through Patch Antennas	29
3.3.1 Inductive Coupling Measurements	32

3.3.2	Capacitive Coupling Measurements	35
3.4	Conclusion	38
4.	CONCLUSION	39
4.1	Patch Antennas Made Out of TCOs	39
4.2	Coupled Feeds for Meshed Patch Antennas	40
4.3	Future Work	41
	REFERENCES	42

LIST OF FIGURES

1.1 USUsatl - TOROID [1]	3
1.2 Meshed see-through copper antenna [16]	3
1.3 Proximity coupled feed for a patch antenna	4
2.1 Illustration quantum states of materials (a) simplified band diagram for a transparent conductor oxide with conduction band doping (b) (E,k) energy band structure of a doped TCO	11
2.2 Typical plot of a TCO conductivity as a function of wavelength for frequencies ranging from the visible spectrum through the microwave regime.	13
2.3 Illustration of patch antenna charge and current density distribution	16
2.4 Cross section of a microstrip current at microwave frequencies where (a) $W/h \ll 1$ and (b) $W/h \gg 1$	16
2.5 Optical transmission coefficient for $\lambda_0 = 550 \text{ nm}$ light and electron mobility $\mu_e = 50 \text{ cm}^2\text{V}^{-1}\text{s}^{-1}$ for various electron densities N_e	19
2.6 Optical transmission coefficient for $\lambda_0 = 550 \text{ nm}$ light and electron mobility $\mu_e = 100 \text{ cm}^2\text{V}^{-1}\text{s}^{-1}$ for various electron densities N_e	20
2.7 Microstrip patch efficiency e_r for various antennas above a PEC ground with resonant frequencies between 100 MHz to 10GHz for electron mobility of $\mu_e = 50\text{cm}^2\text{V}^{-1}\text{s}^{-1}$	21
2.8 Microstrip patch efficiency e_r for various antennas above a PEC ground with resonant frequencies between 100 MHz to 10GHz for electron mobility of $\mu_e = 100\text{cm}^2\text{V}^{-1}\text{s}^{-1}$	22
2.9 Meshed see-through microstrip patch antenna	23
3.1 Geometry of a co-planar electromagnetically coupled feed	27
3.2 Direction of polarization for different rotation rectangular microstrip patches	27
3.3 Cross section of a coupled microstrip line and antenna.	28
3.4 Equivalent circuit of a coupled microstrip line and antenna with (a) a current maxima coupled configuration and (b) a voltage maxima configuration.	29
3.5 Power absorpotion of the patch antenna as a function of feed separation S	30
3.6 Picture of meshed and solid patch antennas resonant at 2.4 GHz	31
3.7 Radiation pattern of E-Plane in dB of solid patch antenna fed through a passive feed with an inductive configuration	33

3.8	Radiation pattern of E-Plane in dB of meshed patch antenna fed through a passive feed with an inductive configuration	34
3.9	Radiation pattern of E-Plane in dB of solid patch antenna fed through a passive feed with a capacitive configuration	36
3.10	Radiation pattern of E-Plane in dB of meshed patch antenna fed through a passive feed with a capacitive configuration	37

LIST OF TABLES

2.1	Conductivity of TCO for electron mobility μ_e for electron densities N_e	19
2.2	Electron mobility and density of various TCOs	21
2.3	Simulation vs. empirical results for antenna radiation efficiency e_r with $\sigma = 2.6 \times 10^5 S/m$, $h = 2.3 mm$ and $W = 7.5 mm$	22

ACKNOWLEDGEMENTS

I would like to thank my friend, advisor and mentor, Dr. Cynthia Furse, for all of her support throughout my academic career at the University of Utah. Her ability to transform the hardest subjects into simple and easy concepts is unmatched.

I would also like to thank my wife, Larissa Saberin, for her patience, love and dedication. I would not be here if it wasn't for her unwavering support. I would like to thank my parents and sister for their love, support and for showing me that hard work pays off.

I would like to thank my fellow graduate colleague, James Nagel, for all the good times, intense science and politics discussions, Latex and Matlab coaching. I wouldn't be able to do this in such short time without your help. Finally, I would like to thank my friends for all the patience, support and help throughout my life.

CHAPTER 1

INTRODUCTION

1.1 Transparent Antennas

Satellites have always played an important role in space. Their contributions for space research, extended global communications and surveillance have been instrumental for the advancement of the information age. As part of the effort to create this outer space network, satellites have evolved from simple transmitters to complex systems that incorporate a myriad of technologies into a single location. Cost and weight are always key issues for successful satellite deployment. Groups of researchers and budget-tight companies employ smaller and cheaper satellite solutions that are usually custom made for a specific application. These small satellites, such as USUsat1, shown in Fig. 1.1, have created a constant demand for cheaper systems that do more with less [1]. Limitations on the size of these small satellites leave barely enough room for solar cells, which are necessary to power the satellite. This repeatedly impedes the placement of other external elements such as antennas. Without the required surface area for topical antennas, often complex and failure prone antennas that must be deployed in orbit are used. This adds substantially to cost and labor hours as well as the potential for failure.

Two solutions have arisen to mitigate the difficulty of solar cell and antenna integration. The first solution entails the placement of a slot antenna on the back side of the solar cell [14]. This solution has been proven effective if custom built solar cell antennas are assembled for small satellites, but is not viable if the small satellite is being built from off-the-shelf components. The second solution suggests the placement of meshed see-through copper antennas, such as the one

seen in Fig 1.2, on top of the solar cell [21]. See-through meshed antennas are still in the early research phase, but show some promise as transparent antennas.

This thesis considers another type of transparent antenna that can be integrated on an off the shelf solar panel. Indium Tin Oxide (ITO) antennas on solar cell panels. ITO antennas have been used for various types of antenna applications including [8], [12] and [4]. ITO has been shown to have high optical transparency while maintaining effective RF conductivity [8]. These properties could potentially make ITO a good candidate for the application of optically transparent antennas for solar cells, but many of these antennas have failed to meet expectations for efficiency while retaining transparency. This thesis will analyze the effect of ITO materials on patch antenna design in Chapter 2. The tradeoff between optical transparency and electrical conductivity will be evaluated for a wide range of frequencies. Methods to better predict the skin effects on a patch antenna and their impact on antenna efficiency are also described. The assessment of these tradeoffs and effect of ITO parameters for antenna design is the first contribution of this thesis.

Another challenge for ITO and meshed patch antenna design is how to feed the antennas. Soldering a copper feed line to the ITO antenna melts the ITO, making the antenna worthless. A proximity feed, shown in Fig. 1.3 and described in detail in Chapter 3, is used instead. The full understanding of that feed and its effects on efficiency gain, polarization and antenna matching is the second major contribution of this thesis.

It is important to note that the application of transparent antenna design concepts is not limited to TCOs, but can be applied to other emerging technologies that utilize materials with lower conductivity values, such as conducting fabrics.

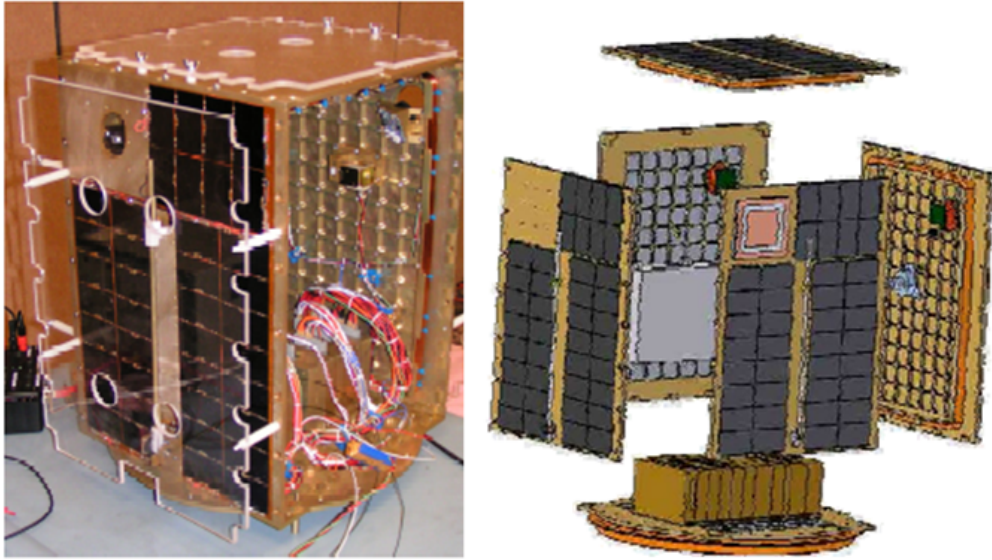


Figure 1.1. USUsatl - TOROID [1]

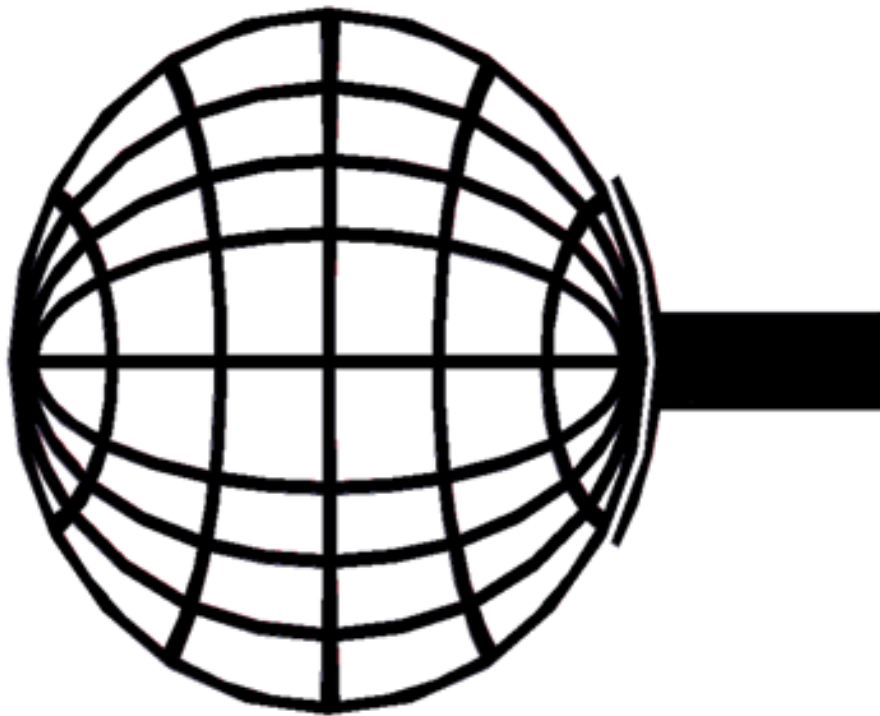


Figure 1.2. Meshed see-through copper antenna [16]

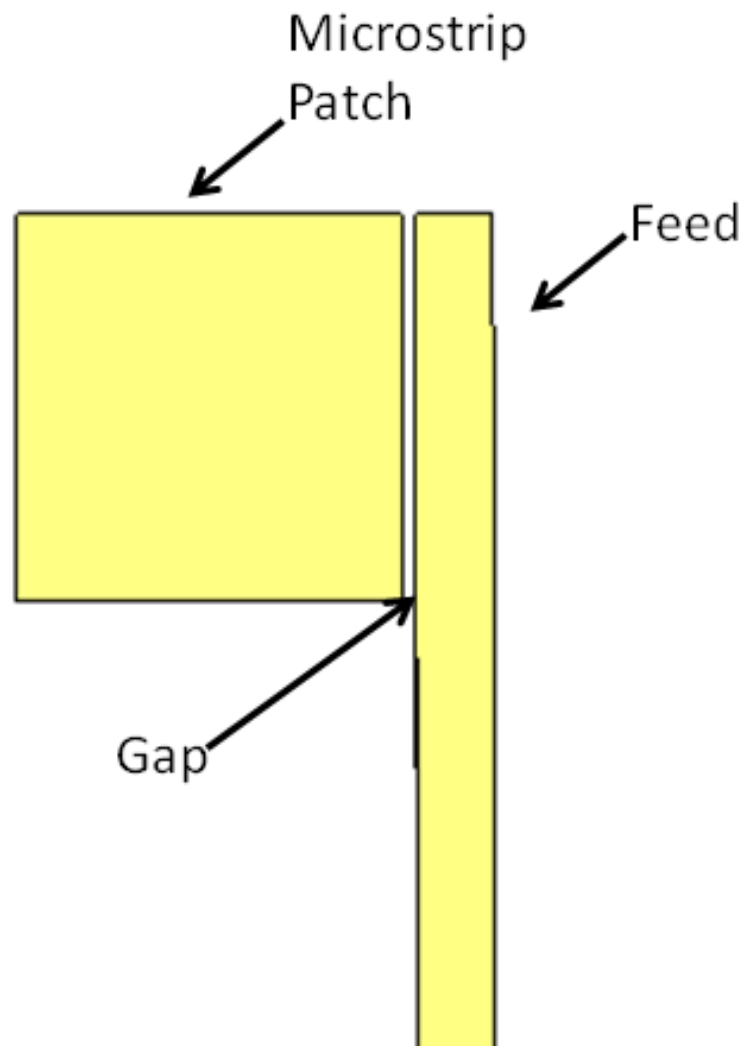


Figure 1.3. Proximity coupled feed for a patch antenna

1.2 Transparent Antenna Design

1.2.1 ITO (Indium Tin Oxide) Antennas

Previous experiments have been conducted to determine the feasibility of using optically transparent materials such as ITO for antenna design [2]. Monopole and patch antennas have been made with ITO [8]. It was found that patch antenna radiators are not as effective or as as monopole antennas. Efficiency is controlled by how much current runs on the ITO imperfectly conducting antenna surface. In [8] PIFA (Planar Inverted F Antenna) was found to have a higher radiation resistance, because it behaves like a cavity and excites a larger current on the whole patch. The trapezoidal monopole requires less current to be excited on its surface and therefore is more efficient [8]. None of the previous designs have been placed on a solar cell.

[12], [4] and [8] have found that ITO antennas optical transparency is inversely proportional to the sheet resistivity and therefore ITO antennas have poor conductivity. This results in a tradeoff between transparency and efficiency for ITO antennas for solar cell applications. This tradeoff is evaluated in Chapter 2.

Chemical spray deposition, DC sputtering and RF sputtering are a few of the methods used for performing ITO deposition [4]. The University of Utah's Nanofab has a DC sputtering machine that was used to sputter the ITO antennas on glass substrates similar to solar cells for this thesis.

1.2.2 Meshed Patch Antennas

An alternative to antennas made of transparent materials are meshed antennas. Although the optical transparency of meshed antennas is typically lower than ITO antennas, meshed antennas have higher efficiency and overall gain [21].

Studies have been conducted at Utah State University, and new techniques for improvement of meshed patch antenna transparency and efficiency have been developed. Utah State University

researchers have been successful in obtaining 80% transparency and 50% efficiency using the meshed structure [21].

1.2.3 Integrated Solar Cell Antennas

Integrated solar cell antennas have been developed with great success. They provide virtually no obstruction or degradation to the solar cell and still are able to maintain high gains and radiation efficiency [14].

The SOLANT (SOLar ANTennas) design incorporates a slot antenna in the ground plane of a solar panel [14]. With this design solar panels are able to function at their maximum capacity because the antenna blocks no light to the solar panel. The SOLANT design was able to achieve gains of up to 30 dBi.

The integrated slot antenna design requires antennas to be custom fabricated, which is cost prohibitive for small satellites.

1.3 Feeding Methods for Transparent Antennas

1.3.1 Direct Microstrip Feed

The direct microstrip feed is the oldest and most traditional feeding technique that works well when the antenna can be printed on a single layer. For patch antenna designs, quarter wave transformer or inset fed techniques have been developed to provide better matching [2].

These feeding techniques do not work well with meshed antennas. Visible feed lines on top of solar cells shadow the energy generating cells. Furthermore, the possibility of integrating meshed printed patch antennas onto the line feed is difficult due to the fragile and unreliable bond of mesh lines and feed. For the reasons mentioned above, alternative techniques must be employed for optimally feeding of mesh antennas.

1.3.2 Coupled Microstrip Feed

An alternative approach to the direct feed described above is using a coupled feed. A passive feed works with a rectangular patch element that is capacitively or inductively coupled to a microstrip feed line. The capacitive coupling depends on the dimensions of the patch as well as the width of the gap between the patch and the feed [2]. At higher frequencies, this arrangement has very low field coupling and bandwidth.

Proximity fed antennas are a good alternative to more common direct feed methods due to the absence of direct connection between the antenna and the feed line. This type of coupled feed mitigates some difficulties between meshed copper bonding and frees up more solar cell area for increased power efficiency.

1.3.3 Contributions

The major contributions of this thesis is to provide the reader with a better understanding of transparent conducting oxides (TCOs) so that antenna design tradeoffs can be implemented and improved upon. The study conducted on Chapter 2 will be published as an invited paper on the IEEE Antennas and Propagation Magazine. Also a major contribution from Chapter 3 is the implementation of electromagnetically coupled feeds for meshed antennas, this work will be published on the IEEE Transactions on Antennas and Propagation journal.

CHAPTER 2

TRANSPARENT PATCH ANTENNAS

2.1 Introduction

Transparent conductive materials have been prepared with oxides of tin, indium, zinc and cadmium [7]. These transparent conducting oxides (TCO) are employed in a wide spectrum of applications such as solar cells, electromagnetic shielding and touch-panel controls [7]. Notably, there has been little commercial application of TCOs in antenna design. Attempts have been made to create transparent patch antennas for automobile windshields and solar cells [8][21][12][4][18]. Many papers on this subject express the inability to achieve high gains (> 2 dB) [4] and reduced efficiencies of microstrip antennas compared to antennas that are not near a ground plane [8], such as a dipole in free space. Previous transparent antenna research offers little insight into the use and limitations of TCO antennas in general, and what range of conductivity and transparency can be expected from today's materials and how that impacts antenna performance for different frequency bands. This chapter explores those trade offs and discusses the implementations for antenna design now and as TCO materials mature.

In order to better understand the importance of these material science constraints and how they impact transparent antenna design, this chapter also looks at transparent conductors in a language that can be understood by antenna engineers. In this effort we examine various issues that plague microstrip patch antenna design using thin film transparent conductors. These design difficulties include skin depth losses introduced by the requirement of thin TCO depositions for high optical transparency. Furthermore, ground effect losses present in patch antennas further

aggravate the loss due to skin effects. Both of these issues coupled with the relatively low conductivity of TCOs [13], (approximately 8×10^5 S/m for indium tin oxide ITO) can cause significant increases in surface resistance of the microstrip patch and resultant lower efficiency. Taking into consideration all of these effects, this work will evaluate 1) the necessary components and requirements of a transparent material for antenna design, 2) the type of losses associated with thin film depositions due to ground and skin effect losses in microstrip patch antennas, and 3) design considerations to mitigate antenna surface resistance and improve efficiency. The first item is addressed by a thorough explanation of TCO material physics, which will illustrate how to manipulate free electron doping and electron mobility to improve transparency and maximize conductivity. The second item introduces an empirical equation to approximate surface resistance due to skin and ground losses. The third item evaluates expected optical transparency and radiation efficiency of today's TCOs and those that we may hope to see in the future. It may also be noted that many of the concepts in this chapter apply to the design of antennas with other imperfectly conducting materials such as fabric or thread.

2.2 Transparent Conductors

Transparent conductors such as ITO, belong to the family of oxides ($In_2O_3 : Sn$) that possess high optical transparency ($> 80\%$ at 550 nm wavelength) and good electrical conductivity ($\approx 10^5$ S/m) [13]. These seemingly opposing characteristics of transparent and conducting oxides are possible through some of the governing laws of modern physics. Before we are able to understand the science behind transparent conductors, it is necessary to simplify the electron conduction model through the Drude model. The Drude model [3] is a physics model that attempts to explain the electron transport properties with the application of kinetic theory. This model exists under three major assumptions:

1. Electrons are treated as classical particles within a free-electron approximation. In the absence of an external electromagnetic field each electron is assumed to move in a straight line. In the presence of a field each electron is assumed to obey Newton's law of motion.
2. Electrons move freely only between collisions. These collisions are instantaneous events that abruptly alter the velocity of an electron, much like colliding balls on a pool table.
3. An electron experiences a collision, resulting in an abrupt change in its velocity, with a probability per unit time of $1/\tau$. The time between these two collisions is known as the mean free path time τ .

In order to accept these Drude model assumptions, the quantum interactions of electrons in energy bands warrants the adjustment of the electron rest mass m_e to a new adjusted value m^* . This m^* provides an approximation of the effective electron mass and allows the calculations to use the acceleration and force of a mass-spring system $\mathbf{F} = m^*\mathbf{a}$. In other words, when applying the usual equations of electrodynamics to charge carriers in a solid, we must use altered values of particle mass. This accounts for most of the influences of the crystal lattice, so that electrons can be treated as nearly free carriers (Drude model) [19] in our future calculations.

The effective mass of an electron in a band with a given (E, \mathbf{k}) relationship is $m^* = \hbar^2 / \frac{d^2 E}{d\mathbf{k}^2}$. This electron mass is inversely related to the second derivative of the energy band curve (E, \mathbf{k}) , shown in Fig. 2.1 (b), and proportional to \hbar , the reduced form of Planks constant. In the case of Fig. 2.1, the electron energy E is parabolic with the wave vector \mathbf{k} , this parabolic relationship is what determines the effective mass m^* of the TCO. Literature [13] suggests that $m^* \cong 0.35m_e$ for a TCO such as ITO.

In an effort to understand the duality of optical transparency and microwave conductivity of TCOs, a deeper understanding of TCO doping is required. In the case of ITO, simultaneous

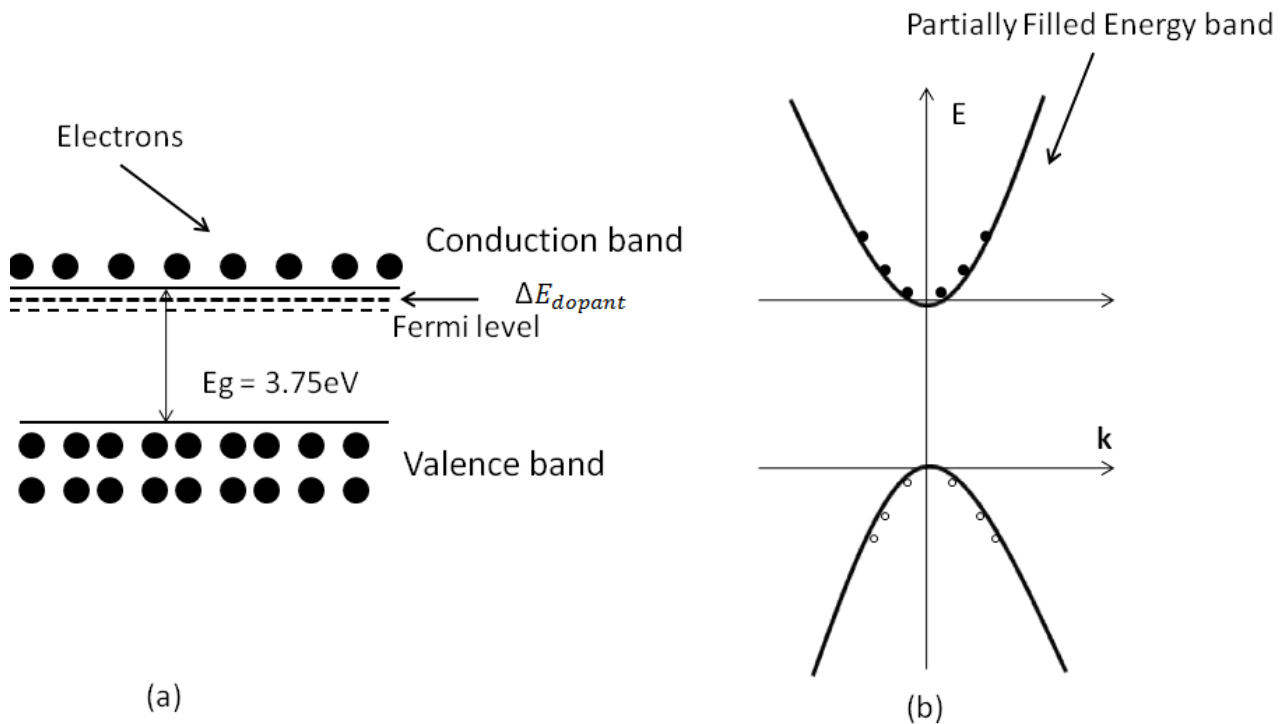


Figure 2.1. Illustration quantum states of materials (a) simplified band diagram for a transparent conductor oxide with conduction band doping (b) (E,k) energy band structure of a doped TCO

transparency and conductivity is possible due to the chemical doping of tin for indium or by the presence of oxygen impurities in indium oxides. With enough doping it is possible to create a degenerate gas of free carrier absorption in far-infrared frequencies where the material is transparent at visible wavelengths. These free carriers produce, high electronic conductivity at microwave frequencies [13]. Under this free electron model, created by conduction band doping, the optical and conductive properties may be simply described by using Drude's model [19], presented in the following paragraph.

With Drude's model it is possible to use Maxwell's equations to model the conductivity and permittivity of the TCO as a function of frequency. In this case it is well known that a local current density \mathbf{J} within a material follows

$$\nabla \times \mathbf{H} = j\omega\epsilon\mathbf{E} + \mathbf{J}, \quad (2.1)$$

this equation can be separated into a conduction current $\mathbf{J}_c = \sigma_{DC}\mathbf{E}$ and a displacement current $\mathbf{J}_d = (j\omega\epsilon_r\epsilon_0 + \sigma_d)\mathbf{E}$ where we solve the frequency dependent sigma with the displacement current term into

$$\sigma_d = \frac{1}{(1 + j\omega\tau)}, \quad (2.2)$$

where $\tau = \epsilon/\sigma$. We can now combine both the conduction current conductivity σ_{DC} with the displacement current conductivity σ_d to form a single effective frequency dependent conductivity $\sigma(\omega)$

$$\sigma(\omega) = \left(\frac{N_e q^2 \tau}{m^*} \right) \left(\frac{1}{1 + j\omega\tau} \right) = \frac{\sigma_{DC}}{1 + j\omega\tau}, \quad (2.3)$$

where N_e is the electron density of the TCO in m^{-3} , q is the electron charge in Coulombs and DC conductivity is

$$\sigma_{DC} = \frac{N_e q^2 \tau}{m^*}. \quad (2.4)$$

Since $\nabla \times \mathbf{H} = \mathbf{J} + j\omega\epsilon(\omega)\mathbf{E}$, the Drude model of the frequency dependent dielectric can be considered. Separating the real and imaginary parts of $\epsilon(\omega)$ yields,

$$\epsilon_1(\omega) = \epsilon_\infty - \frac{\omega_p^2 \tau^2}{1 + \omega^2 \tau^2}, \quad \epsilon_2(\omega) = \frac{1}{\omega} \left(\frac{\omega_p^2 \tau}{1 + \omega^2 \tau^2} \right), \quad (2.5)$$

where ϵ_∞ is the high-frequency relative permittivity of the conducting material. It is found that when $\epsilon_1(\omega_p) = 0$, the plasma frequency ω_p of a conducting material can be determined as

$$\omega_p = \left(\frac{N_e q^2}{\epsilon_\infty \epsilon_0 m^*} - \frac{1}{\tau^2} \right)^{\frac{1}{2}}. \quad (2.6)$$

From Equation (2.6) it is noted that the electronic relaxation time τ , also referred to as electron mobility, $\mu_e = q\tau_0/m^*$ has very little influence on the plasma frequency, leaving the

electron density N_e as the dominant factor that determines the plasma frequency of the TCO, illustrated in Fig. 2.2. In order to maximize transmission of the whole visible electromagnetic spectrum ($\lambda_{visible} = 400 \text{ nm to } 700 \text{ nm}$) through the material, the plasma frequency must be below the lowest visible wavelength ($\frac{2\pi}{\omega_p} < \lambda_{visible}$). If the plasma frequency is set to be barely below the lowest visible wavelength it is found that the electron density N_e must satisfy the following relationship,

$$N_e < \frac{4\pi^2 \epsilon_\infty m^*}{\mu_0 q^2 \lambda_{visible}^2}, \quad (2.7)$$

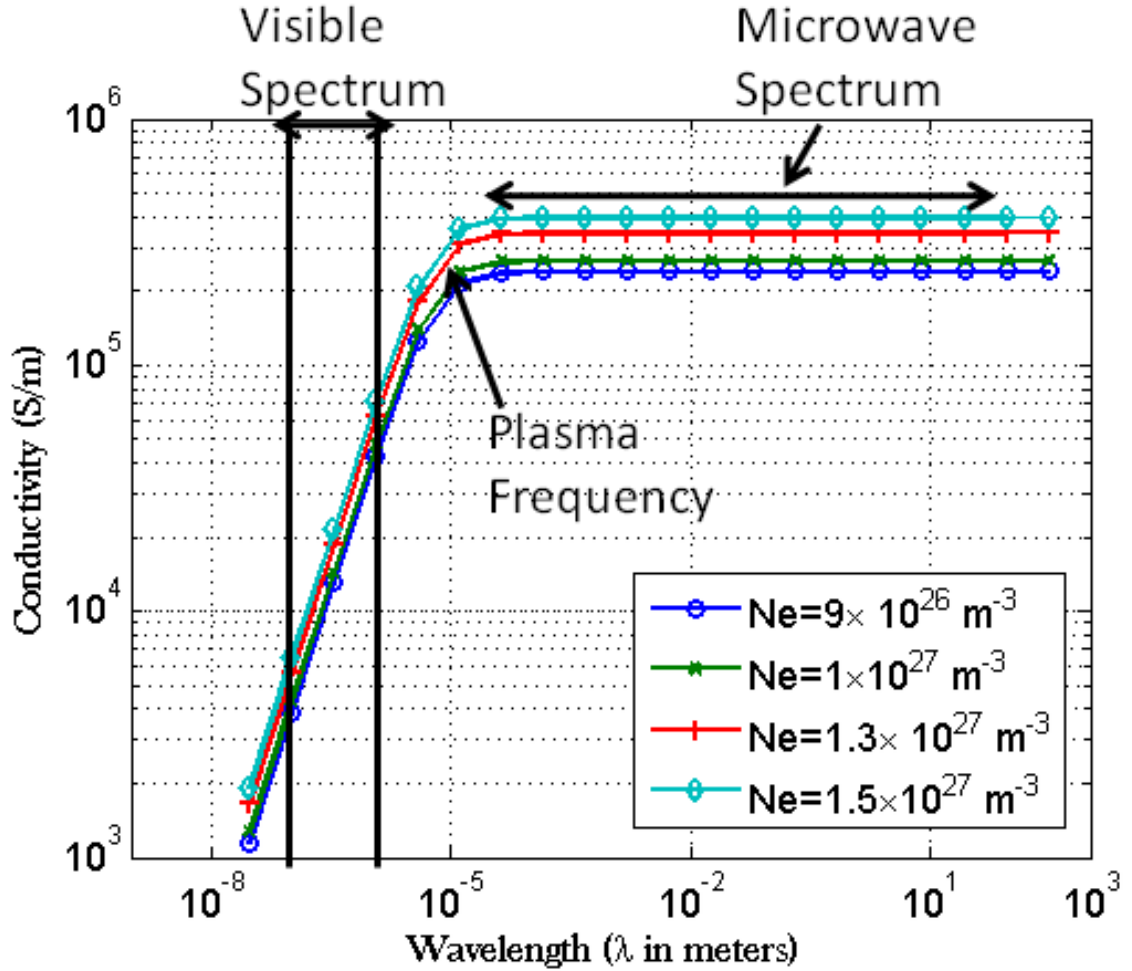


Figure 2.2. Typical plot of a TCO conductivity as a function of wavelength for frequencies ranging from the visible spectrum through the microwave regime.

where, μ_0 is the magnetic permeability of free space. Equation (2.7) will serve as a guideline for the doping of free electrons in the transparent material. To allow a small margin of error for visible transmission it is recommended that we use a material with a plasma wavelength of just over $\lambda_p = 1 \mu\text{m}$ (near-infrared). The power reflection for optical frequencies $R(\omega)$ of a uniform TCO deposition (dielectric slab) is defined as

$$R(\omega) = \left| \frac{\sqrt{\epsilon(\omega)} - 1}{\sqrt{\epsilon(\omega)} + 1} \right|^2. \quad (2.8)$$

For frequencies much lower than the plasma frequency ω_p the transmission coefficient $T(\omega) = 1 - R(\omega)$ tends to be close to 0. Alternatively, for frequencies above the plasma frequency the transmission coefficient increases and $\lim_{\omega \rightarrow \infty} = 1$, depending on the TCO's permittivity values. This transmission coefficient is also dependent on the amount of absorbed energy as it travels through the lossy dielectric slab(TCO). The amount of absorbed energy is determined by the electromagnetic skin depth δ , which constrains the electromagnetic wave energy loss as it travels through a thickness t of the TCO. The transmission of light through a TCO is well approximated by

$$T(t) \cong e^{\left(\frac{-2t}{\delta}\right)}. \quad (2.9)$$

The dual characteristic of light absorption and microwave energy conduction of the TCO yields two separate equations that determine the skin depth at frequencies where the TCO is a good conductor but not very transparent $\omega_p > \omega$, case 1, and where the TCO is transparent $\omega_p < \omega$, case 2, as illustrated below:

Case 1, where $\omega_p > \omega$, $\omega\tau \ll 1$:

$$\epsilon_2 \approx \frac{\omega_p^2 \tau}{\omega} \gg |\epsilon_1|, \quad \delta \approx \left(\frac{2}{\omega \mu \sigma} \right)^{\frac{1}{2}} \quad (2.10)$$

Case 2, where $\omega_p < \omega$, $\omega\tau \gg 1$:

$$\epsilon_2 \approx \frac{\omega_p^2 \tau}{\omega^3 \tau} \ll |\epsilon_1|, \quad \delta \approx \frac{2m^* \omega^2 \tau}{Z_\infty q^2 N_e} \quad (2.11)$$

where we assume that $\omega < \frac{E_g}{\hbar}$, $\epsilon_1 \approx \epsilon_\infty$, $Z_\infty = \frac{377}{\sqrt{\epsilon_\infty}} \Omega$ and μ is the magnetic permeability of the TCO. In the second case where the transparency is proportional to the electron mobility μ_e . Furthermore, an increase in mobility will ultimately increase both the transparency and conductivity of the TCO. It is also important to observe that an increase in the free electron mass m^* will have the same effect. Therefore, the choice of a TCO for antenna design is determined by the material's electron density N_e , free electron mobility μ_e and free electron mass m^* ultimately dictated by the TCO's (E,k) band structure shape.

2.3 Skin and Ground Effects on Thin Film Microstrip Antennas

Unlike dipole antennas in free space, current distribution on the microstrip patch can vary significantly when the width (W) of the patch is much greater than height (h), $W/h \gg 1$, as seen in Fig. 2.3 and Fig. 2.4. This change in current distribution is better understood with the help of the *field equivalence principle* (Huygens' principle) [2]. Under a condition where $W/h \gg 1$ we can assume that the current on the top of the patch (\mathbf{J}_t) is much smaller than the one on the bottom (\mathbf{J}_b). Under this assumption, the cavity model provides further simplification by considering the current density on the top of the microstrip patch \mathbf{J}_t to be zero [2]. Moreover, because the ground plane is near the patch, the magnetic current density is maximized on the walls of the cavity, thus doubling the magnetic current density on the perfect current density conducting walls.

The increase in magnetic current density in the cavity model results in an increased current distribution on the bottom surface of the microstrip, as seen in Fig. 2.3 and Fig. 2.4, where the

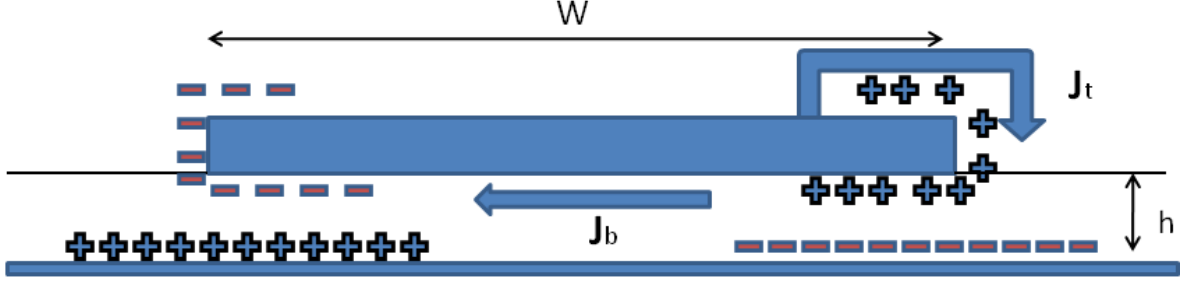


Figure 2.3. Illustration of patch antenna charge and current density distribution

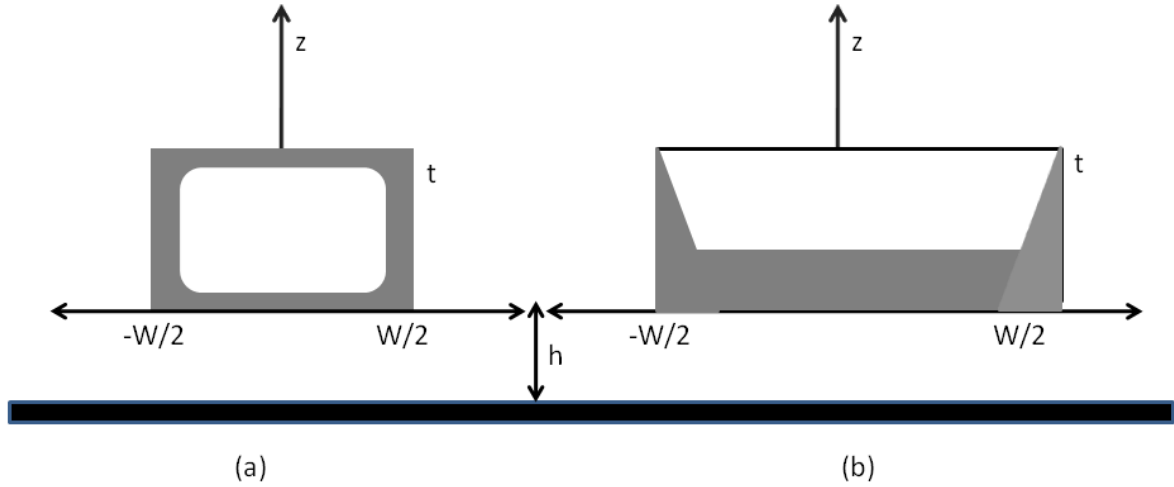


Figure 2.4. Cross section of a microstrip current at microwave frequencies where (a) $W/h \ll 1$ and (b) $W/h \gg 1$

current density distribution of a microstrip is compared to its width to height ratio [6].

This situation implies that the AC resistance of the strip, R_s , at large width to height ratios can be as much as twice that of smaller ratios. [6]

$$R_s = R_s, \text{ if } \frac{W}{h} < 1, \quad R_s = 2R_s, \text{ if } \frac{W}{h} \gg 1 \quad (2.12)$$

When using TCOs, thin film deposition on the order of 100 nm to 2 μm , is necessary to keep transparency high. However, when depositions are thinner than skin depth $\delta = \sqrt{\frac{2}{\sigma\omega\mu}}$ the surface resistance dramatically increases as a function of thickness t , compounded by the doubling of the

surface resistance. This relationship is demonstrated if we assume an exponential current density distribution over the patch $J_x = \sigma E_{x0} e^{(-t/\delta)}$ and the surface resistance of the rectangular shaped patch antenna can be defined by initially defining the current through a surface extending from 0 to infinity in the z direction and width W in the y direction, we integrate $I = \int J_x dS$ where $dS = dy dz$ [23]. Then we have

$$I = \int_{z=0}^t \int_{y=0}^W \sigma E_{x0} e^{-\alpha z} dy dz = \left[\frac{-W \sigma E_{x0}}{\alpha} e^{-\alpha z} \right] = W \sigma E_{x0} \delta (1 - e^{-\alpha z}) \quad (2.13)$$

$$I_s = W \sigma E_{x0} \left(1 - e^{-\frac{t}{\delta}}\right), \quad V_s = E_{x0} L, \quad (2.14)$$

where L is the length of the patch. In this case, the surface resistance can be defined as

$$R_s \approx \frac{L}{\sigma W \delta \left(1 - e^{-\frac{t}{\delta}}\right)}, \quad \text{if } \frac{W}{h} < 1, \quad (2.15)$$

or

$$R_s \approx 2 \frac{L}{\sigma W \delta \left(1 - e^{-\frac{t}{\delta}}\right)}, \quad \text{if } \frac{W}{h} \gg 1. \quad (2.16)$$

It is worth noting that both Equations (2.15) and (2.16) provide an empirical approximation of the surface resistance caused by the skin effect losses. Due to an extreme current density deformation at thicknesses $t \ll \delta$ a full wave numerical solver may be necessary to properly predict skin and ground effects and hence surface resistance for transparent patch antennas. Additionally, Equations (2.15) and (2.16) do not account for additional sources of loss such as surface roughness, lossy substrate, lossy ground planes, etc.

2.4 Analysis of TCO Effects on Patch Transparency

In order to better understand the effects of electron mobility μ_e and carrier concentration N_e , on TCO transparency, we will analyze ITO, a widely used TCO for use in antenna design.

Electron mobility and carrier concentration can be controlled through changing oxygen and argon concentrations. Annealing can improve transparency as well as conductivity [7]. Various deposition methods such as DC sputtering, RF sputtering, thermal deposition, spray pyrolysis and pulsed laser deposition may be used for thin film deposition of ITO on a substrate [7]. These methods can influence the TCO deposition rate, uniformity and oxide doping. TCO's may be deposited on a variety of optically transparent substrate materials such as glass and clear fluorocarbon (FEP) film.

Typical values for ITO permittivity and effective electronic mass are $\epsilon_\infty \approx 4.0$ and $m^* = 0.35m_e$ [13]. Electron mobility on high quality ITO films can reach values of $\mu_e \approx 50 \times 10^{-4} m^2V^{-1}s^{-1}$, with a DC scattering time $\tau_0 \approx m^*\mu_e/q \approx 10^{-14}$ s. Drude empirical approximations suggest that the electronic relaxation time is $\tau \approx 3.3 \times 10^{-15}$ s. For our example antenna a glass substrate with a dielectric of $\epsilon_r = 6.0$ and height $h = 2.3$ mm, is used. The ground plane is copper and is considered to be a perfect electric conductor (PEC). In Fig. 2.5, we find that optical transmissions for ITO are high (greater than 50%) at deposition thicknesses of $t \leq 1\mu m$ or below. The optical transparency of the microstrip patch is not greatly affected by the electron density, but much better transmission of light is achieved if we increase the electron mobility to $\mu_e = 100 \times 10^{-4} m^2V^{-1}s^{-1}$ as seen in Fig. 2.6. The decay of optical transparency is greatly reduced below an electron density of $N_e < 1 \times 10^{27} m^{-3}$, keeping optical transparency above 60%. Although transparencies improve with lower electron densities, the electrical conductivity suffers. Increasing electron mobility, on the other hand, increases both the transparency and conductivity. Table 2.1 shows that conductivity doubles as electron mobility doubles. The same relationship is observed for the increase of electron density. The near linearity of this relationship gives $\mu_e \propto \sigma$ and $N_e \propto \sigma$.

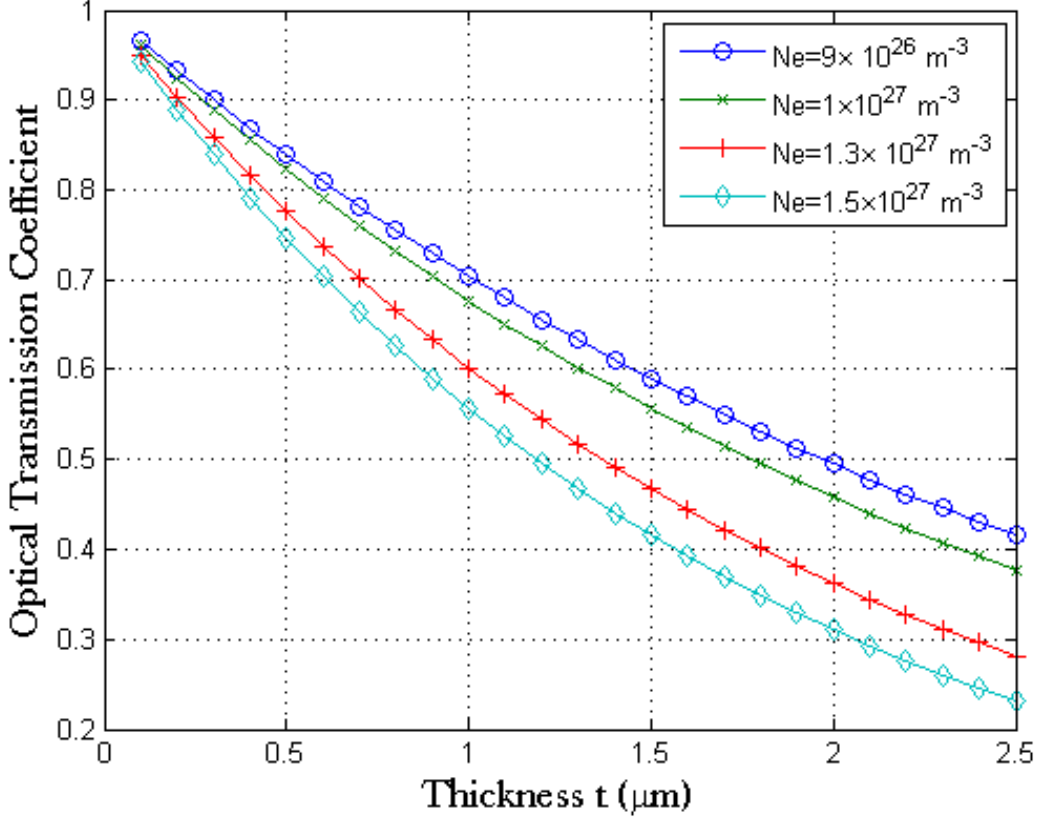


Figure 2.5. Optical transmission coefficient for $\lambda_0 = 550 \text{ nm}$ light and electron mobility $\mu_e = 50 \text{ cm}^2\text{V}^{-1}\text{s}^{-1}$ for various electron densities N_e

Table 2.1. Conductivity of TCO for electron mobility μ_e for electron densities N_e

	$N_e = 9 \times 10^{26} \text{ m}^{-3}$	$N_e = 1.5 \times 10^{27} \text{ m}^{-3}$
$\mu_e = 50 \text{ cm}^2\text{V}^{-1}\text{s}^{-1}$	$2.4 \times 10^5 \text{ S/m}$	$4.0 \times 10^5 \text{ S/m}$
$\mu_e = 100 \text{ cm}^2\text{V}^{-1}\text{s}^{-1}$	$4.8 \times 10^5 \text{ S/m}$	$8.0 \times 10^5 \text{ S/m}$

2.5 TCO and Antenna Design

In the following figures, rectangular microstrip patch antennas were designed to be resonant from a range of 100 MHz to 10 GHz with an input impedance of $R_a = 50\Omega$ by varying their width and length. The radiation efficiency in this case is calculated as $e_r = \frac{R_a}{R_a + R_s}$ and is shown in Fig. 2.7 for electron mobility of $\mu_e = 50 \text{ cm}^2\text{V}^{-1}\text{s}^{-1}$ and shown in Fig. 2.8 for $\mu_e = 100 \text{ cm}^2\text{V}^{-1}\text{s}^{-1}$. The deposition thickness t of the ITO deposition is $1.2\mu\text{m}$ in order to achieve transparencies of

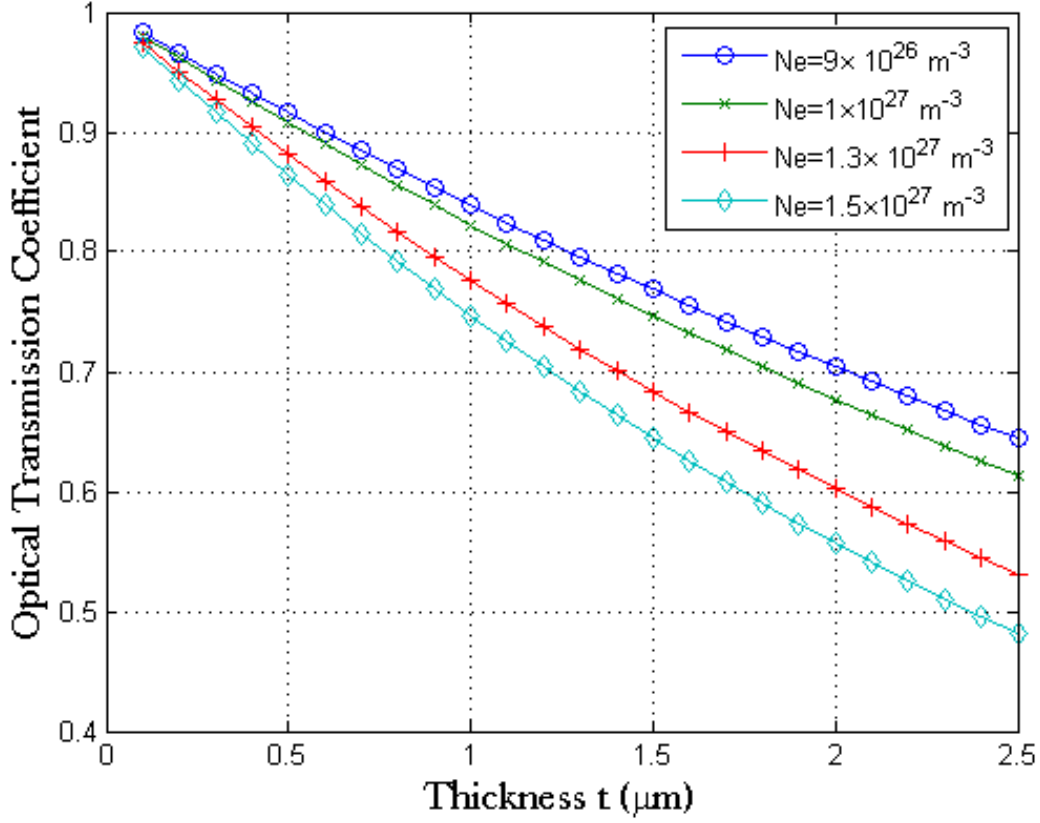


Figure 2.6. Optical transmission coefficient for $\lambda_0 = 550 \text{ nm}$ light and electron mobility $\mu_e = 100 \text{ cm}^2 \text{V}^{-1} \text{s}^{-1}$ for various electron densities N_e

50% to 68%, seen in Fig. 2.5 and transparencies of 70% to 80%, seen in Fig. 2.6.

These antennas have very poor radiation efficiencies at frequencies below 2GHz. Fair efficiencies (more than 40%) are achieved for frequencies above 5GHz. It is important to note that electron mobility above $\mu_e = 100 \text{ cm}^2 \text{V}^{-1} \text{s}^{-1}$ is very hard to achieve and further materials development should be done to improve the electron mobility of TCOs, literature [13] suggests that novel materials such as titanium doped indium oxide could provide higher than $\mu_e = 50 \text{ cm}^2 \text{V}^{-1} \text{s}^{-1}$ mobility. Table 2.2 gives a sample of different TCO materials and their respective μ_e and N_e . If the ground plane is also transparent, the radiation efficiency e_r would drop substantially due to ground surface resistance R_g , so mobility would become even more critical.

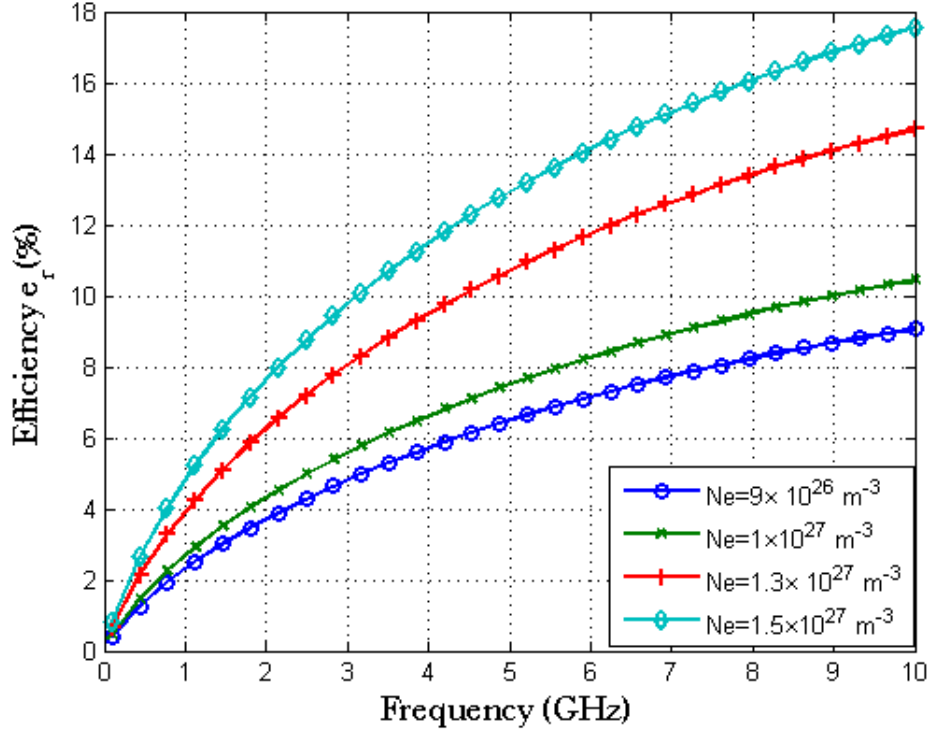


Figure 2.7. Microstrip patch efficiency e_r for various antennas above a PEC ground with resonant frequencies between 100 MHz to 10GHz for electron mobility of $\mu_e = 50 \text{ cm}^2 \text{ V}^{-1} \text{ s}^{-1}$

The empirical results from Equation(2.16) were compared to full wave numerical simulation results using CST Microwave StudioTM. Good agreement is seen, as shown in Table 2.3.

One method of improving efficiency involves the placement of high conductivity materials, such as copper, in areas of high current density [18]. This technique claims to improve transparent

Table 2.2. Electron mobility and density of various TCOs

Transparent Conductor	Mobility μ_e ($\text{cm}^2 \text{ V}^{-1} \text{ s}^{-1}$)	Density N_e (m^{-3})
Indium Tin Oxide [13]	45	4×10^{26}
Antimony Tin Oxide [10]	9.7	1.26×10^{26}
Titanium Indium Oxide [22]	80	8×10^{26}
Gallium Zinc Oxide [20]	13	1×10^{26}

Table 2.3. Simulation vs. empirical results for antenna radiation efficiency e_r with $\sigma = 2.6 \times 10^5 S/m$, $h = 2.3 \text{ mm}$ and $W = 7.5 \text{ mm}$

Antenna thickness t	Empirical e_r	Simulation e_r
$t = 0.5 \mu m$	6.4%	10.0%
$t = 1.2 \mu m$	28.3%	25.8%
$t = 3.0 \mu m$	70.3%	53.2%

patch antenna efficiencies up to 30% and could be used to improve TCO antenna efficiencies.

An alternative to TCO antennas is meshed antennas [21] made from non-transparent conductors, seen in Fig. 2.9. These antennas are able to achieve effective transparencies by reducing the metallic area while still retaining much of the electrical size and performance of a solid patch. See-through patches are known to achieve transparencies of up to 80% while maintaining

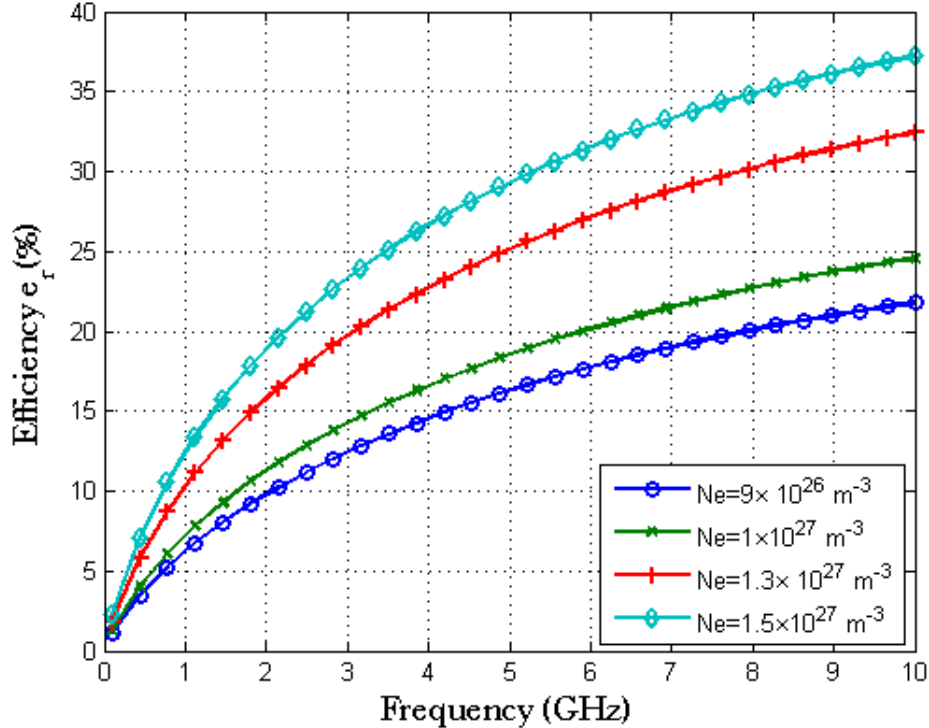


Figure 2.8. Microstrip patch efficiency e_r for various antennas above a PEC ground with resonant frequencies between 100 MHz to 10GHz for electron mobility of $\mu_e = 100 \text{ cm}^2 \text{ V}^{-1} \text{ s}^{-1}$

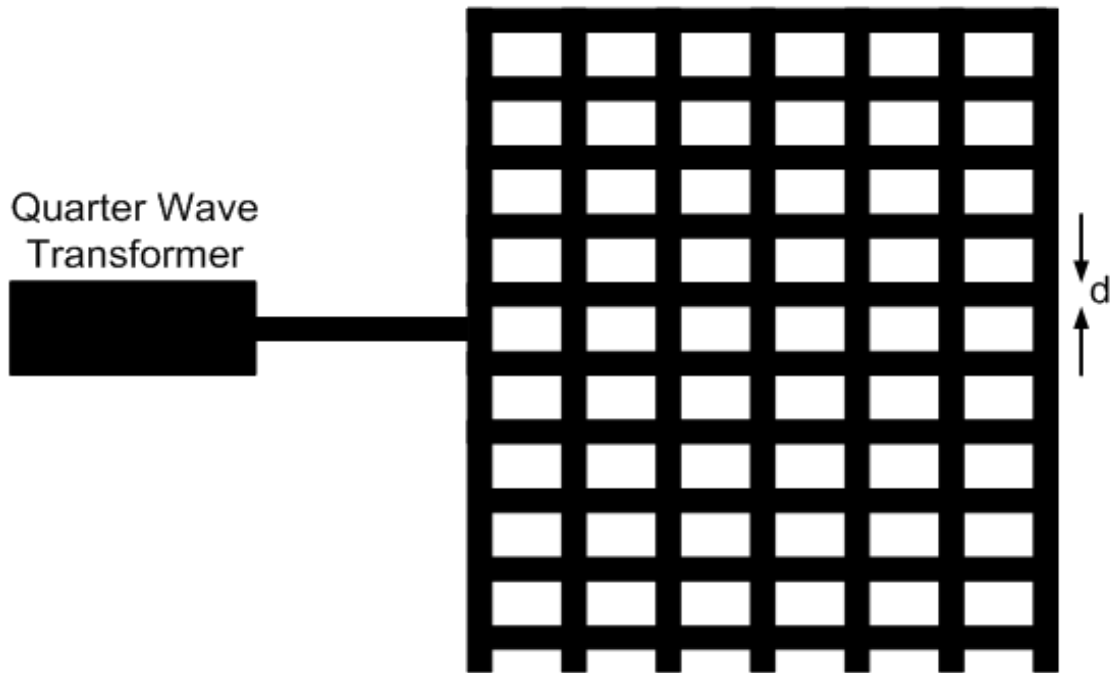


Figure 2.9. Meshed see-through microstrip patch antenna

approximate radiation efficiencies of up to 60% [21]. It is also important to note that the ground and skin depth effects are minimal for these antennas, due to copper's high free electron density ($N_e = 8.46 \times 10^{28} \text{ m}^{-3}$) and electron mobility of ($\mu_e = 44 \times 10 \text{ cm}^2 \text{ V}^{-1} \text{ s}^{-1}$). Unlike antennas made out of TCOs, see-through antennas do not require thin depositions and can even be deposited inexpensively with metallic ink-jet printing [16].

2.6 Conclusion

Transparent and conductive antennas are limited by intrinsic properties. Factors such as thin film depositions smaller than $2\mu\text{m}$ create severe skin effect losses that deeply influence antennas at microwave frequencies. When TCO materials are used for microstrip patch design, the losses might increase by a factor of $4\times$, caused by a deformation of the current density around the patch and ground. The feasibility of a high efficiency lies in the TCO's material properties that

seem to be restricted by intrinsic limitations of TCOs. however, if higher electron mobilities μ_e ($> 100\text{cm}^2\text{V}^{-1}\text{s}^{-1}$) is achieved then perhaps transparent antennas might turn into a viable commercial product.

CHAPTER 3

PASSIVE FEED METHOD FOR MESHED MICROSTRIP PATCH ANTENNAS

3.1 Introduction

Recent advancements in transparent patch antenna designs have enabled the placement of antennas above the surface of solar cells [21] and on transparent surfaces, such as automobile windows [5]. Optically transparent antenna designs can be made of see-through meshed forms [21] or out of transparent materials such as Indium Tin Oxide (ITO) [15]. Much of the difficulty of feeding these antennas is attributed to the poor bonding of conductive materials, such as copper, to feed meshed see-through patch antennas. Furthermore, when implementing antenna arrays the difficulty of feeding optically transparent microstrip patches without blocking the power harvesting area of a solar cell can also be a challenge. Notwithstanding these shortcomings, a co-planar electromagnetically coupled passive feed method for transparent antennas is presented. This feed is presented as an inexpensive and easy implementation of a feed line that can be used topically on solar cells or other transparent surfaces without blocking its light transmission.

3.2 Co-planar Electromagnetically Coupled Feed

A common configuration of a passive coupled feed is addressed as a two layer structure where the feed line is placed underneath the antenna [2]. In the case of feeding antennas placed on an existing structure such as a solar cell, coupled feeds must be modified to feed the antenna from its side, as shown in Fig. 3.1.

3.2.1 Co-Planar Coupled Feed

The co-planar feed consists of a microstrip patch with feed located near its edge, separated by a gap S , seen in Fig. 3.1. The proximity coupling is mainly due to fringing fields spilling out of the edge of the feedline or the magnetic field surrounding the feedline. When a feedline of length λ is fed with an alternating current the line creates a standing wave with current maxima at $\lambda/4$ and $3\lambda/4$ [11] [9]. This concentration of current maxima enables the inductive coupling of a microstrip patch antenna. This is accomplished by magnetic field vectors perpendicular to the feedline direction of current flow. From this induced magnetic field a surface current is induced in the y direction of the patch, seen in Fig. 3.2.

Inversely, if the open circuited end of the feed is extended by $\lambda/4$ the feedline is able to shift the current standing wave by 90° ($\lambda/4$) thus creating a voltage standing wave at the middle of the microstrip patch, with voltage maxima at $\lambda/4$ and $3\lambda/4$. This voltage maximum induces charges at the edge of the patch antenna, thus exciting a surface current with a direction x , seen in Fig. 3.2. This feed uses a capacitive coupling configuration.

The following section focuses on the on the influences of the microstrip feed distance to the antenna and polarization switching capabilities.

3.2.2 Inductive and Capacitive Coupling of a Passive Feed

The second parameter to be studied in side coupled feeds is the relationship between the gap distance, S , and its effect on magnetic and capacitive coupling, as seen in Fig 3.3. The coupling between the feed and the antenna can be considered as two distinctive circuits, shown in Fig. 3.4. In the case of the placement of current maxima at the center of the patch, shown in Fig.3.2, the equivalent circuit can be compared to inductors that represent the self and mutual inductances, L_s and L_m , shown in Fig. 3.4 (a). When coupling occurs at voltage maxima, shown in Fig. 3.3,

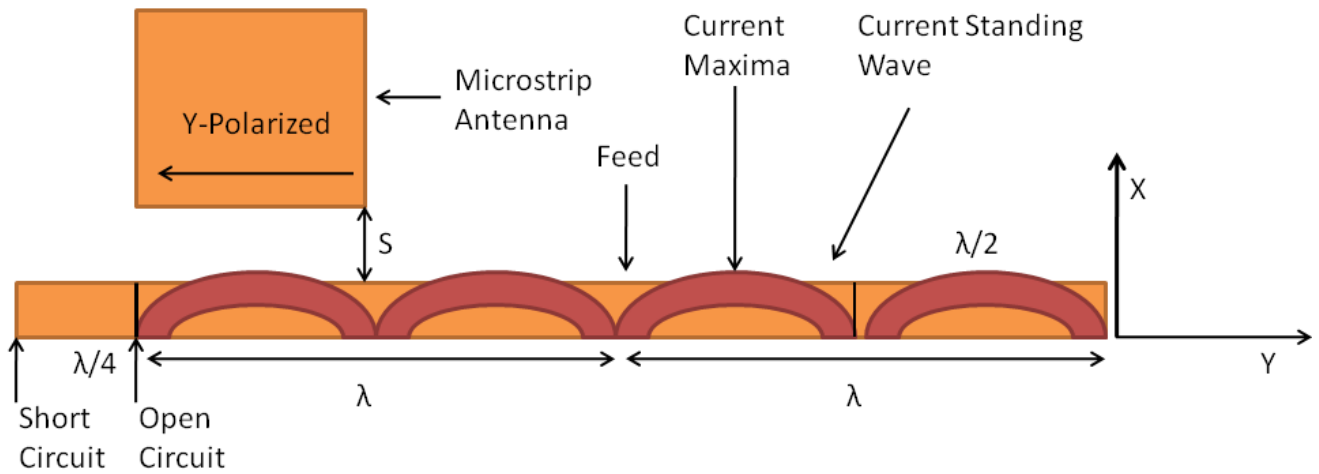


Figure 3.1. Geometry of a co-planar electromagnetically coupled feed

the equivalent circuit can be represented as a mutual and self-capacitance C_m and C_s , shown in Fig. 3.4 (b).

With the presence of inductive coupling the direction of induced current on the patch is parallel to the current on the feed. This causes a y directed polarization when the feed current

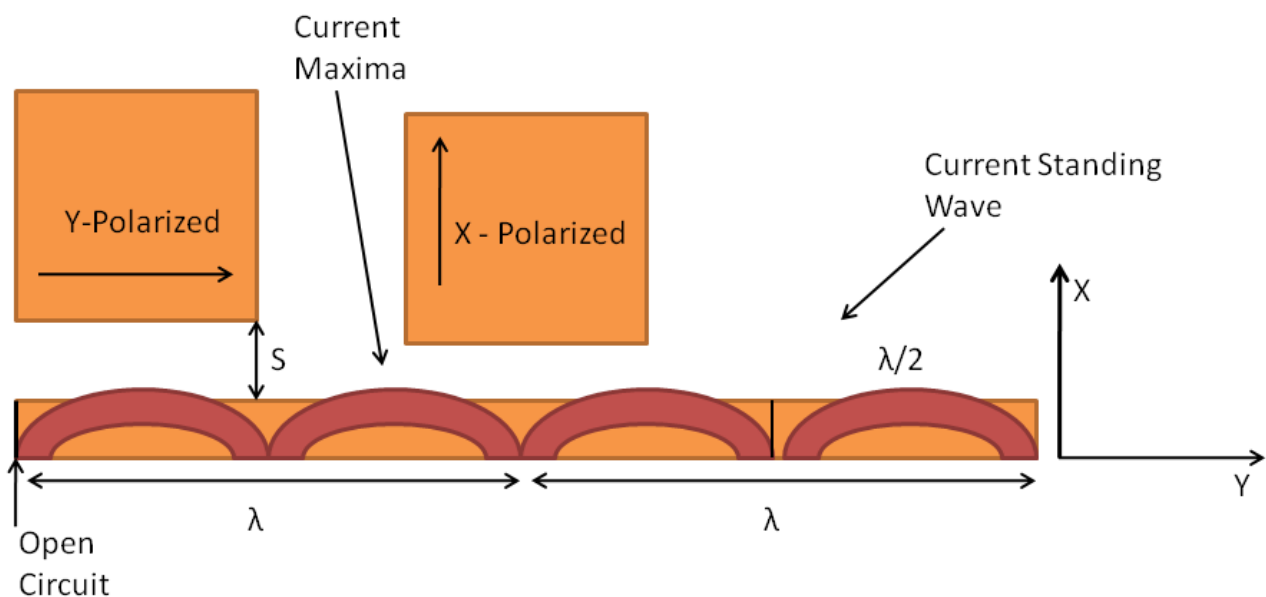


Figure 3.2. Direction of polarization for different rotation rectangular microstrip patches

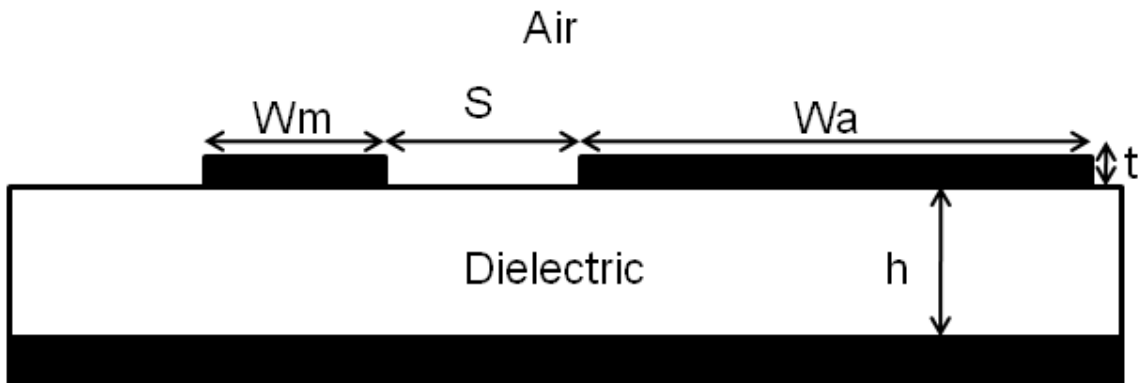


Figure 3.3. Cross section of a coupled microstrip line and antenna.

is y directed. When the passive coupling is capacitive, the current induced on the patch antenna is in the opposite direction of the feedline current. Previous research [17] has demonstrated the ability to obtain polarization diversity with the placement of a PIN diode on the feedline, enabling antennas to work in both x and y linear polarizations or right-hand *RHP* and left-hand *LHP* circular polarizations. It is observed in [17] that when the patch antenna is polarized in the opposite direction of the feedline current, cross-polarization is increased. However, when the feedline current is in the same direction of the current on the patch the cross-polarization is greatly reduced.

3.2.3 Gap Distance and its Effects

For both x and y polarization the gap distance directly influences the power absorption as seen in Fig. 3.5. For power transfer to be maximized at close distances a guideline for gap distance S is to be $\approx 0.005\lambda$. In addition to a decay in power absorption from S , polarization difference can deeply affect power absorption and cross-polarization losses between the patch and the feed. Gap distance can also increase reactive impedances between the feed and the patch in turn modifying the resonant frequency of the feed, seen in Fig. 3.5.

3.3 Meshed See-through Patch Antennas

Another choice for optically transparent antennas is the implementation of meshed see-through antennas [21]. These antennas are patch antennas that have a meshed surface to allow penetration of light through its holes. Meshed patch antennas are able to achieve high transparencies while maintaining high conductivity by using copper as the material of choice for the mesh. Meshed antennas have been able to achieve high transparencies of up to 90% and high

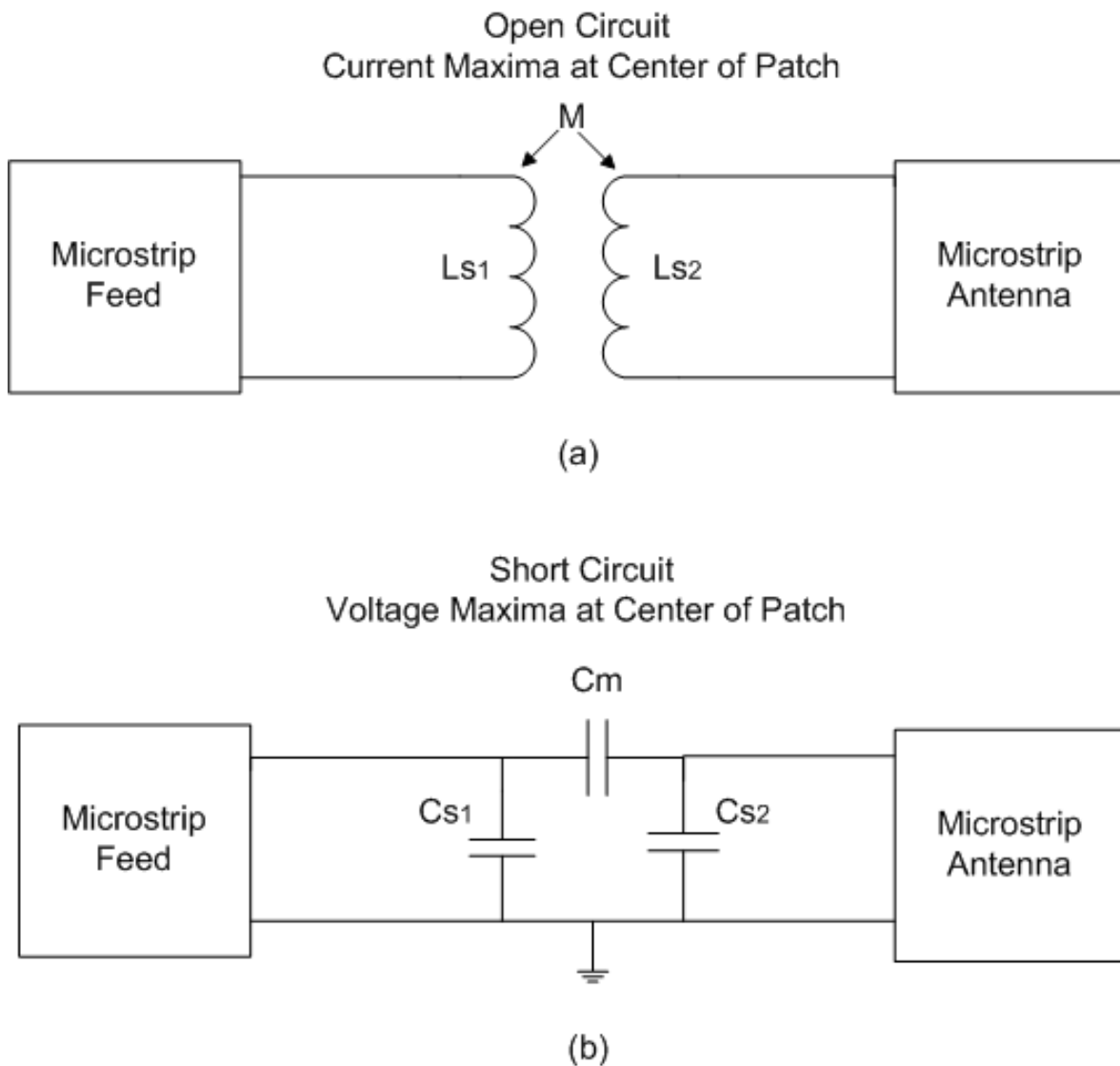


Figure 3.4. Equivalent circuit of a coupled microstrip line and antenna with (a) a current maxima coupled configuration and (b) a voltage maxima configuration

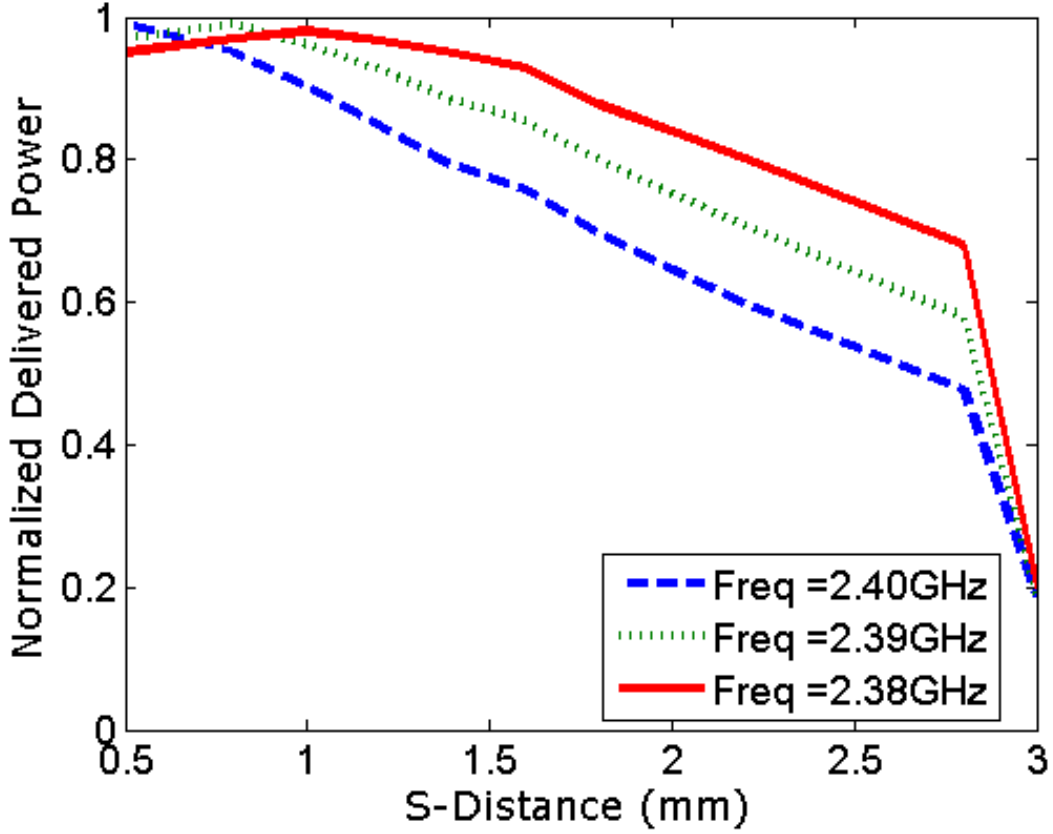


Figure 3.5. Power absorption of the patch antenna as a function of feed separation S

antenna efficiencies of 80% [21], as compared to TCOs where transparencies of 80% have only achieved antenna efficiencies of up to 20%[15] .

The transparency of meshed patch antennas is determined by

$$P_{tran} = \frac{A_{patch} - A_{metal}}{A_{patch}} 100\% = 100\% - metal\%, \quad (3.1)$$

where A_{Patch} is the area of a solid patch, A_{metal} is the total area of the mesh. The transparency of the patch is defined as the percentage of the see-through area of the patch minus the percentage of the metal area.

Meshed see-through antennas are typically fed through the placement of a coaxial feed line at the center of the meshed patch [21]. Other co-planer feeds have been used when feeding meshed

antennas. In this work we have simulated and built four antennas that are electromagnetically fed at a resonant frequency of 2.4 GHz and 2.7 GHz with an input impedance of 50Ω . Two antennas are meshed patch antennas that are coupled through both inductive and capacitive coupling configurations shown in Fig. 3.4 and Fig. 3.6. Two solid copper antennas are placed

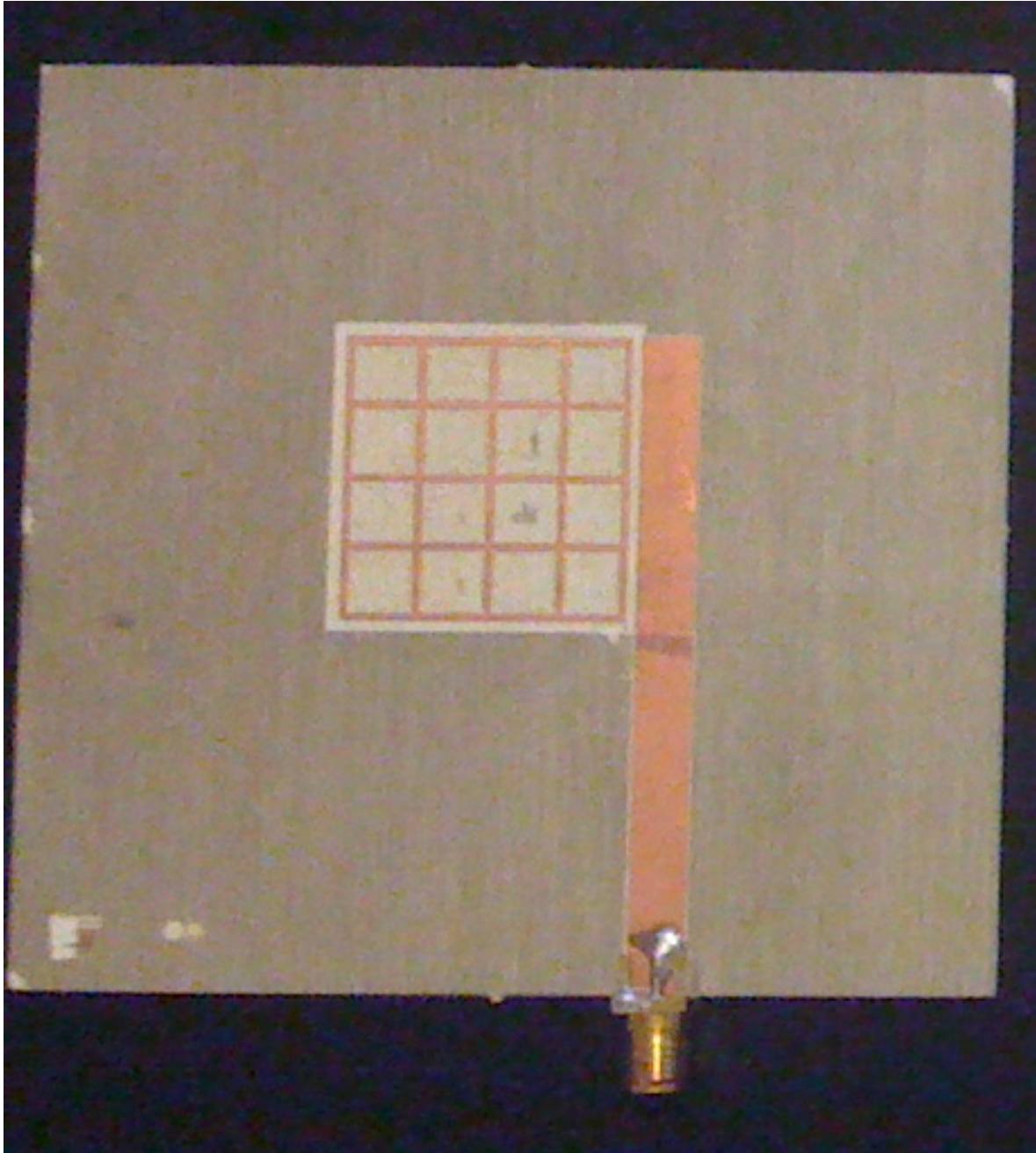


Figure 3.6. Picture of meshed and solid patch antennas resonant at 2.4 GHz

in the same configurations as the meshed antennas for comparison. These patches were built on Rogers RT/Duroid 4350B with $\epsilon_r = 2.33$ and $h = 1.6$ mm for all four antenna designs. In the case of the meshed antennas the transparency was 73% to the solid copper patch antenna, that has a transparency of 0% and seen in Fig. 3.6. The design of the mesh and solid antenna was initially accomplished with the help of CST Microwave Studio simulation software. All four antennas are a 28 mm square. For the mesh antennas the line width is 0.7 mm. All four antennas were simulated using CST microwave studio and good agreement was found between simulation and actual results.

3.3.1 Inductive Coupling Measurements

The inductive feed configuration presented in Fig. 3.4 (a), where the patch is placed at current maxima, was well matched for both solid and meshed patch antennas with insertion losses of -20 dB and -12 dB, respectively. The resonant frequency of the meshed patch was at 2.4 GHz while the solid patch frequency was 2.71 GHz. Fig. 3.7 and Fig. 3.8 show the gains of both antennas. The meshed patch has a gain of 5.69 dB, and the solid patch antenna has a gain at 5.8 dB. The cross-polarization is the main difference between the two antennas. The solid patch has a cross-polarization of -33.57 dB while there was a substantial increase in the cross-polarization of the meshed antenna at -16.95 dB. This increase of cross-polarization on the mesh antenna is controlled by the line thickness of the mesh. Thinner meshes have been shown to improve cross-polarization of mesh antennas, while thicker meshes improve antenna gain [5]. Furthermore, it is explained from [5] that a slight decrease in gain from the meshed antenna is attributed to high currents at the edge of each mesh line.

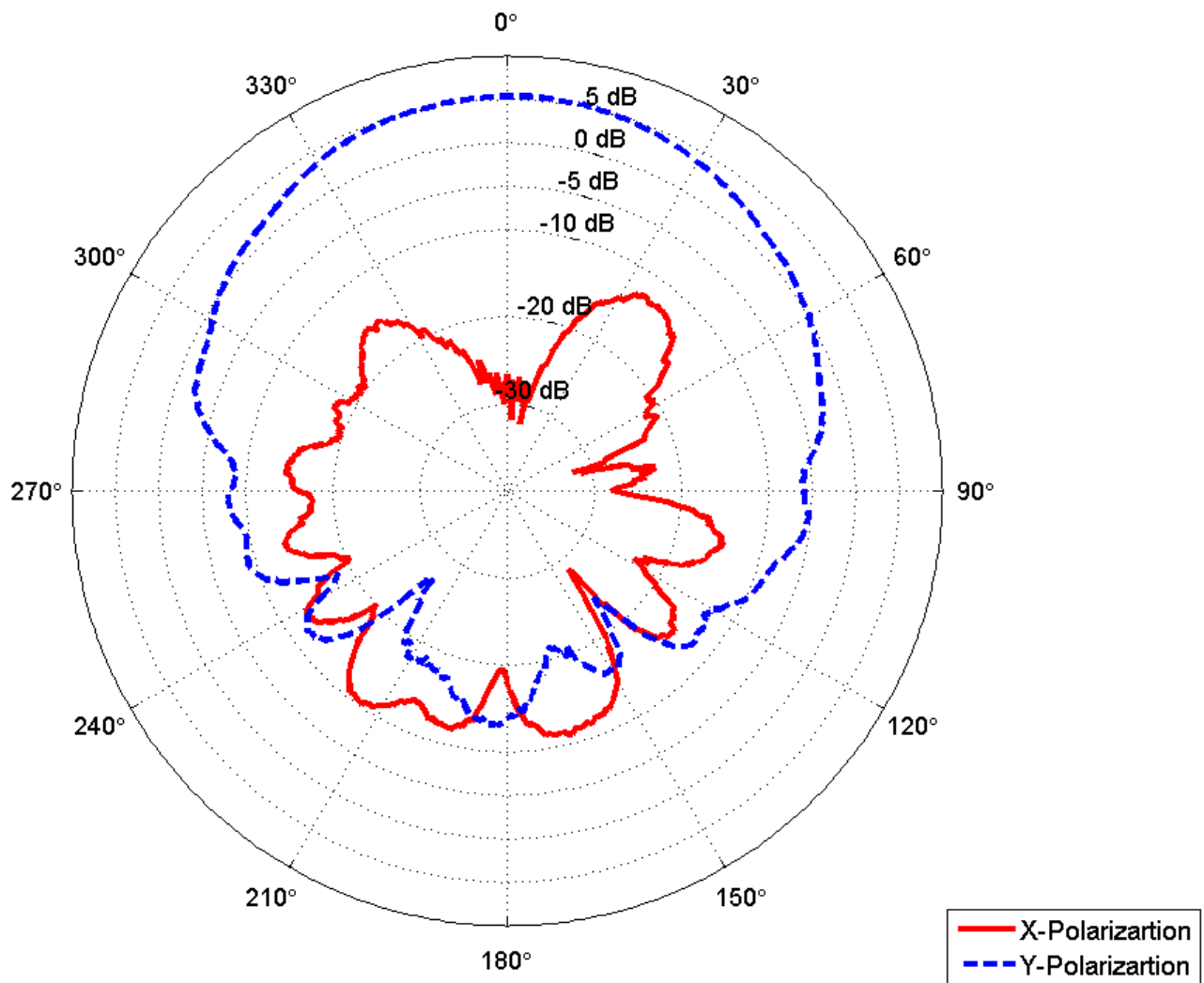


Figure 3.7. Radiation pattern of E-Plane in dB of solid patch antenna fed through a passive feed with an inductive configuration

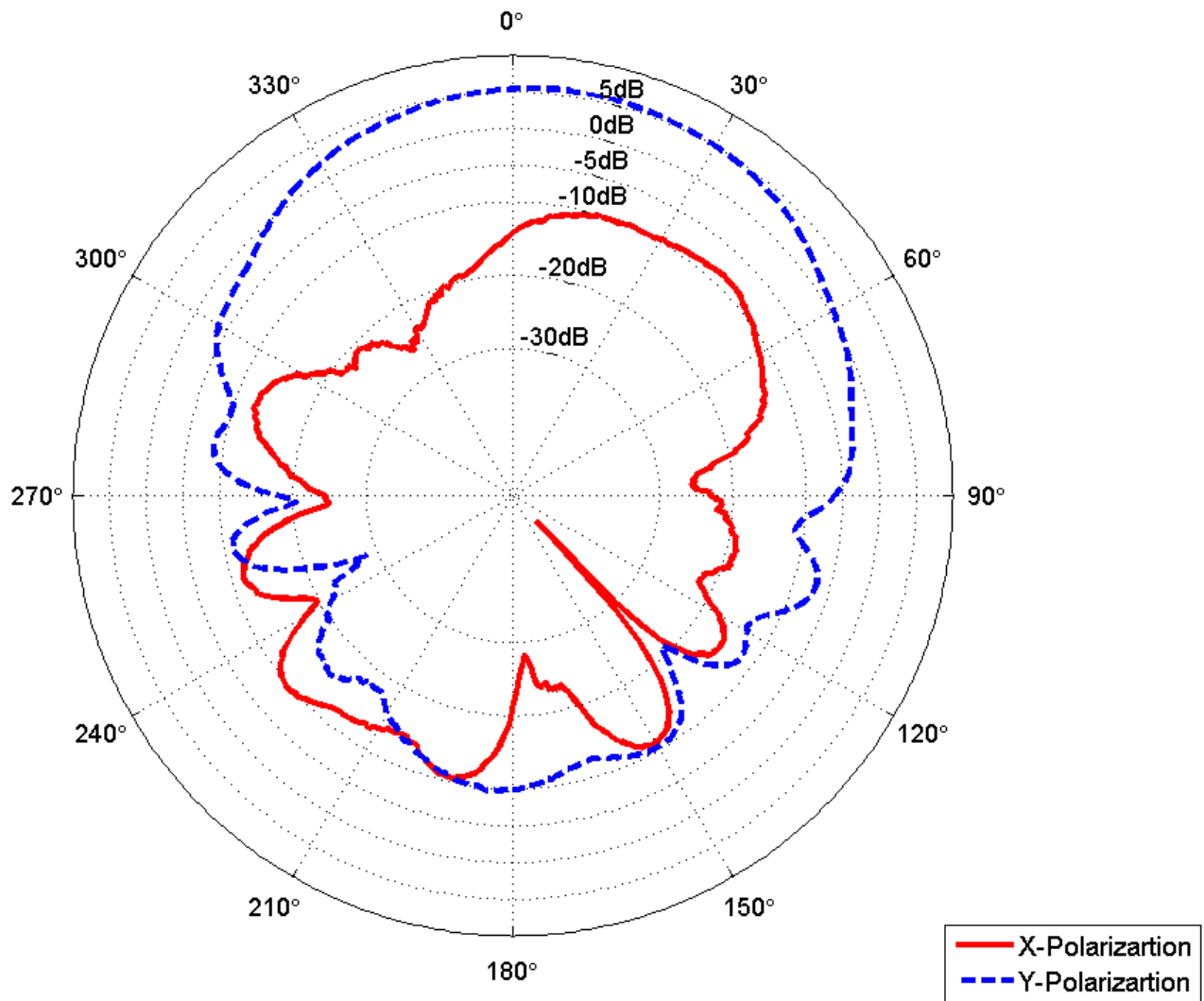


Figure 3.8. Radiation pattern of E-Plane in dB of meshed patch antenna fed through a passive feed with an inductive configuration

3.3.2 Capacitive Coupling Measurements

The capacitive feed configuration presented in Fig. 3.4 (b) was built for both the solid and meshed patch antennas. The resonant frequency for the meshed antenna was very close to 2.4 GHz and the solid patch was 2.7 GHz. The solid patch had a gain of 4.9 dB, seen in Fig. 3.9 and the meshed patch had a lower gain of 4.4 dB, seen in Fig. 3.10. The cross-polarization of the capacitively fed meshed and solid patches is much higher than the inductively fed configurations. The capacitive solid antenna had a cross-polarization of -11.9 dB while the mesh antenna had a much higher value at -5 dB. This result indicates a deep influence of the feed line polarization on the patch's polarization. This is enhanced when the passive feed is applied to meshed antennas.

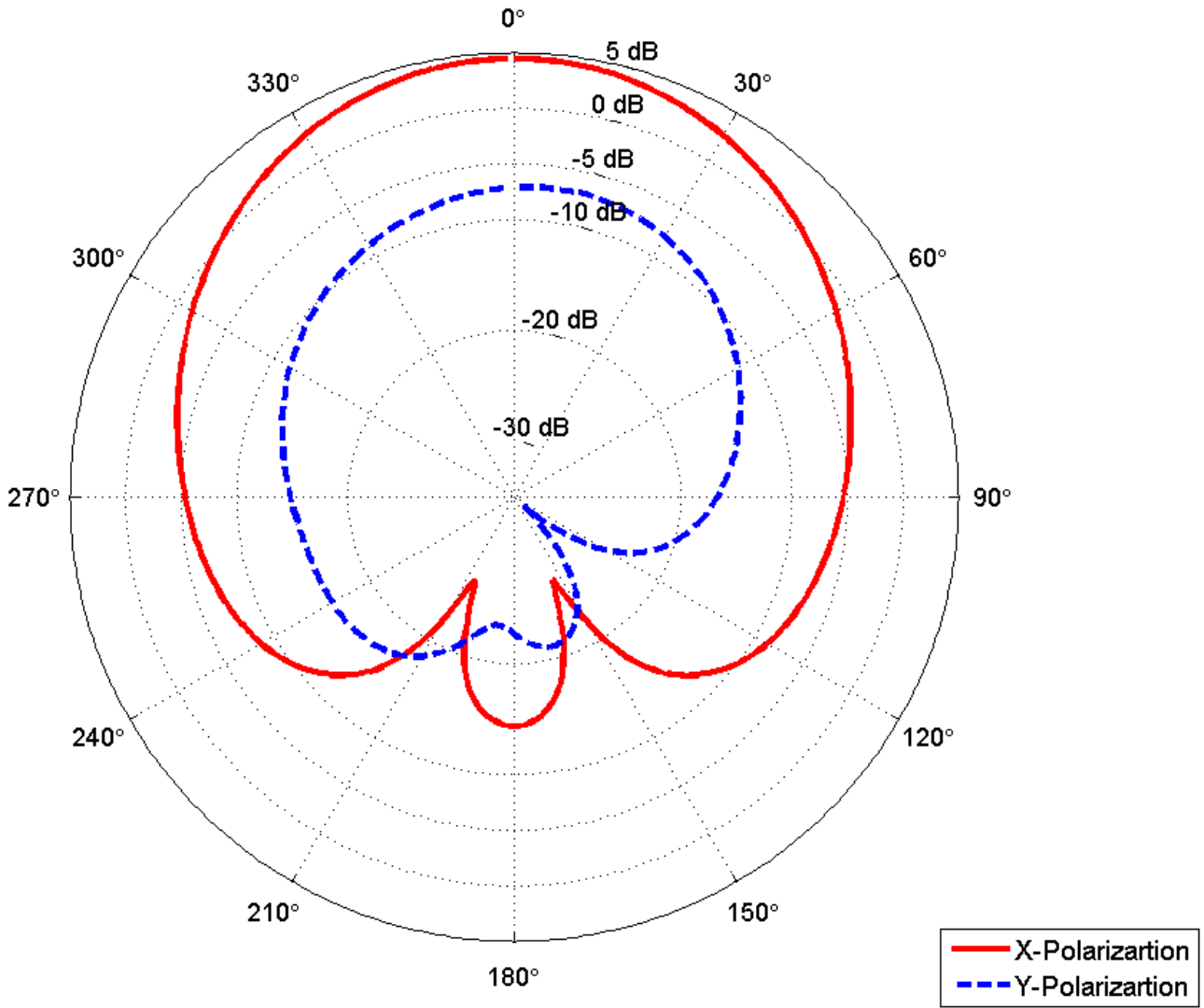


Figure 3.9. Radiation pattern of E-Plane in dB of solid patch antenna fed through a passive feed with a capacitive configuration

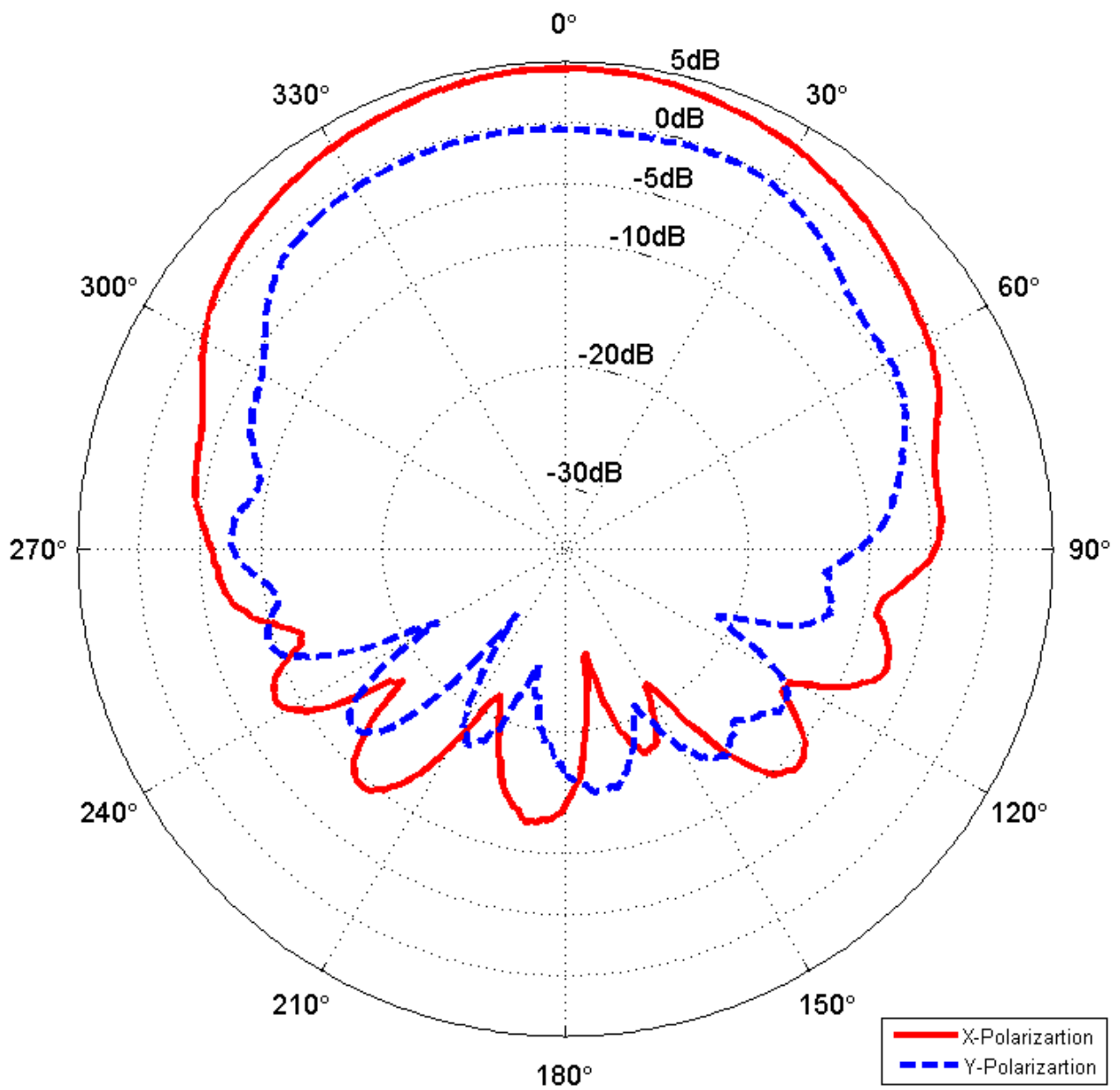


Figure 3.10. Radiation pattern of E-Plane in dB of meshed patch antenna fed through a passive feed with a capacitive configuration

3.4 Conclusion

This chapter has discussed the implementation of electromagnetically coupled co-planar feeds for solid and meshed antennas. Passive feeds can be used to control polarization on an antenna by switching the current maxima and voltage maxima feed position. Also the gap distance between the feed and the antenna can both reduce the coupled power and alter the resonant frequency of the patch antenna, seen in Fig. 3.5. The passive feed did not alter the radiation pattern in both feed configurations. The main influence of the feed on antenna parameters was the cross-polarization levels. Cross-polarization of the solid and meshed patch antennas was -33.57 dB and -16dB, respectively, when placed in the inductive feed configuration. Alternatively, the capacitive feed had a much higher cross-polarization of -11.9 dB for the solid patch and -5 dB for the meshed patch antenna. These higher levels of cross-polarization are due to the contribution of the feed polarization to the overall antenna parameters.

CHAPTER 4

CONCLUSION

4.1 Patch Antennas Made Out of TCOs

The first section of this thesis addressed the shortcomings of current antenna and solar cell integration by studying feasibility of TCO implementation for patch antennas on solar cell panels. Although various studies claim that ITO is a viable material for the implementation of transparent antennas, it is seen in Chapter 2 that this is true only for higher frequencies where skin depth is much smaller and it is important to understand the effects of TCOs as thin film depositions. The properties of each TCO can impact the deposition thickness, transparency and electrical conductivity. These properties ultimately impact antenna efficiency. In the first section of Chapter 2, we learned about the influence of the governing equations of thin film TCO depositions. A study that determines transparency, reflection, absorption and transmission was introduced. Later these properties were used to understand their impact on antenna design. It was seen that thin TCO depositions are the biggest surface resistance factor in the design of transparent antennas. In order to achieve transparent deposition of TCO, they have to be deposited as thin layers of usually 800 nm to 2 μm . These thicknesses introduce high skin effect losses in the microwave regime, 300 MHz to 30 GHz, yielding antenna efficiencies of approximately 10 % to 20 %. An empirical equation was derived to approximate skin effect losses. Furthermore these losses can be generalized by the TCO's electron mobility μ_e and electron density N_e . Reduction of skin depth losses can be mitigated by an increase in electron mobility μ_e . Increased

electron mobility increases electrical conductivity and transparency of TCOs. Unfortunately, TCOs in existence today do not achieve levels of electron mobility to mitigate skin depth losses present in microwave frequencies. Only frequencies above 10 GHz have small enough losses to achieve acceptable efficiency levels while keeping transparencies above 80%. Another factor that influences electrical conductivity of TCO's is electron density N_e . It is seen in Chapter 2 that an increase of electron density will help mitigate some skin losses but unlike electron mobility, it will reduce TCO transparency. Therefore, a set value of electron density is required for improved conductivity. This set value is given in the expression of eq. 2.7. Acceptable ITO patch antenna efficiencies are presently unachievable at microwave frequencies of 300 MHz to 10 GHz, so we introduce some additional techniques that can improve transparent antenna efficiency such as the placement of a material with higher conductivity around areas of the antenna where the current density is high. Alternatives to TCOs were also visited. These alternatives are in the form of meshed patch antennas that can be placed on top of solar cells and cover very little area, thus allowing most of the light on the solar cell to be harvested.

4.2 Coupled Feeds for Meshed Patch Antennas

Chapter 3 introduced the use of co-planar electromagnetically coupled feeds for meshed patch antennas. The use of these types of feeds has not been thoroughly explored in literature. It is demonstrated how the use of coupled feeds is an effective way to feed meshed antennas. A big advantage of these co-planar feeds is the ability to control polarization with minimal bonding to the meshed antenna. These feeds are also viable for transparent antennas made of transparent conducting materials. In the capacitive coupling configuration the meshed patch is placed on the voltage maxima locations of the open ended feed and the polarization is perpendicular to the direction of current flow on the feed line. Alternatively, the inductive coupling is placed

on the current maxima locations of the feed and the polarization is parallel to the direction of current flow on the feed line. This allows a polarization flexibility and even the application of polarization diversity schemes with the placement of a pin diode, discussed in Chapter 3. Gains of up to 5.4 dB were observed for meshed patch antennas, with high cross-polarization (-5 dB) in the capacitive coupling configuration. It was concluded that the high cross-polarization of the feed in the capacitive configuration is due to the direction of current flow on the the feed being orthogonal to the induced current on the coupled patch antenna.

4.3 Future Work

Although this thesis mainly discussed the use of transparent antennas on solar cells, the application for such antennas is not limited to solar cells on small satellites. These transparent antennas can be also used in other areas such as windshields of cars and even as transparent RF circuits. As seen in this thesis, the present state of TCOs has not matured enough to allow the implementation of TCOs in antenna design at microwave frequencies of 100 MHz to 10GHz but can be used at frequencies above 10GHz. This work gives some guidelines and requirements so that antenna engineers and materials scientists can push the boundaries and enable the usage of such materials. The use of transparent TCOs can enable implementation of transparent RF circuits for aviation, transportation and consumer electronics. Once TCOs are improved for use at frequencies of 300MHz to 10 GHz, the implementation of passive feeds presented in this thesis will help with additional challenges such as bonding of TCOs to copper. Furthermore, co-planar coupled feeds can be used to feed materials that are more difficult to bond, such as the feeding of fabric antennas, etc.

REFERENCES

- [1] BAKTUR, R., AND FURSE, C. Transparent solar cell antennas for small satellites. *NSF Proposal Award 0801426*. Utah State University and University of Utah.
- [2] BALANIS, C. *Antenna Theory: Analysis and Design*. Wiley, New York, 1996.
- [3] BOHREN, C. F., AND HUFFMAN, D. R. *Absorption and Scattering of Light by Small Particles*. John Wiley and Sons, New York, 1883.
- [4] BOURRY, M., SARRET, M., AND DRISSI, M. Novel ito alloy for microwave and optical applications. *48th Midwest Symposium on Circuits and Systems 1* (August 2005), 615–618.
- [5] CLASEN, G., AND LANGLEY, R. Meshed patch antennas. *IEEE Transactions on Antennas and Propagation* 52, 6 (June 2004), 1412–1416.
- [6] FARAJI-DANA, R., AND CHOW, Y. L. The current distribution and ac resistance of a microstrip structure. *IEEE Transactions on Microwave Theory and Techniques* 38, 9 (September 1990).
- [7] GORDON, R. Criteria for choosing transparent conductors. *MRS Bulletin* (August 2000).
- [8] GUAN, N., FURUYA, H., DELAUNE, D., AND ITO, K. Antennas made of transparent conductive films. In *PIERS Preceedings Online* (2008), vol. 4.
- [9] HAISHI, K., AND ITOH, K. Proximity feed microstrip antenna. *Electronics and Communications in Japan* 69, 12 (1986).
- [10] HAO, X., MA, J., ZHANG, D., XU, X., YANG, Y., MA, H., AND AI, S. Transparent conducting antimony-doped indium oxide films deposited on flexible substrates by r.f. magnetron sputtering. *Applied Physics A* 75 (2002), 397–399.
- [11] MIYAZAKI, T., AND ITOH, K. Analysis and design on a proximity fed microstrip antenna. In *Proceedings of ISAP 96, Chiba, Japan* (2006), pp. 545–548.
- [12] OUTLEB, N., PINEL, J., DRISSI, M., AND BONNAUD, O. Microwave planar antenna with rf-sputtered indium tin oxide films. *Microwave and Optical Technology Letters* 24, 1 (2000).
- [13] PORCH, A., MORGAN, D. V., PERKS, R., JONES, M., AND EDWARDS, P. P. Electromagnetic absorbtion in transparent conducting films. *Journal of Applied Physics* 95, 9 (May 2004).
- [14] S. VACCARO, J. MOSIG, P. M. Two advanced solar antenna.
- [15] SABERIN, J., AND FURSE, C. Challenges with optically transparent antennas for solar cells. preprint, July 2010.

- [16] SABERIN, J., FURSE, C., YASIN, T., AND BAKTUR, R. Passive feed methods for meshed antennas. preprint.
- [17] SIMBA, A., YAMAMOTO, M., NOJIMA, T., AND ITOH, K. Circularly polarized proximity-fed microstrip antenna with polarization switching ability. *IET Microwave Antennas and Propagation* 1, 3 (2007), 658–665.
- [18] SONG, H. J., HSU, T. Y., SEVENPIPER, D. F., HSU, H., SHAFFNER, J., AND YASAN, E. A method for improving the efficiency of transparent film antennas. *IEEE Antennas and Wireless Propagation Letters* 7 (2008).
- [19] STREETMAN, B., AND BANERJEE, S. *Solid State Electronic Devices*. Pearson Prentice Hall, New Jersey, 2006.
- [20] TIBURCIO-SILVER, A., SANCHEZ-JUAREZ, A., AND AVILA-GARCIA, A. Properties of gallium-doped zno deposited onto glass by spray pyrolysis. *International Symposium on H-Fuel Cell Photovoltaic Systems* 55, 1-2 (1998).
- [21] TURPIN, T., AND BAKTUR, R. Integrated solar meshed patch antennas. *IEEE Antennas and Wireless Propagation Letters* 8 (2009), 693–696.
- [22] VANHEST, M., DABNEY, M., PERKINS, J., AND GINLEY, D. S. Titanium-doped indium oxide: A high mobility transparent conductor. *Applied Physics Letters* 87 (2005).
- [23] WENTWORTH, S. M. *Applied Electromagnetics*. John Wiley and Sons, New York, 2007.